CHALMERS
UNIVERSITY OF TECHNOLOGY

Report No.: EX076/2017

Friction modelling for robotic applications with planar motion

Master's thesis in Systems Control & Mechatronics

IRIS RÖGNER

Department of Electrical Engineering
CHALMERS UNIVERSITY OF TECHNOLOGY
Gothenburg, Sweden 2017

Friction modelling for robotic applications with planar motion
IRIS RÖGNER

Report No.: EX076/2017
Department of Electrical Engineering
Chalmers University of Technology
SE-412 96 Göteborg
Sweden
Telephone +46 (0)31-772 1000

Abstract

Friction is a topic that has been researched since the times of Leonardo da Vinci. The computation of friction allows to derive the force which is needed in order to set robotic devices in motion. To be able to do this, different friction models have been developed. Among these are models that directly connect the velocity to the frictional force such as Coulomb friction and viscous friction, as well as models that use an extended state, for example the model by Dahl, the LuGre model and the elasto-plastic model. However, all these friction models have in common that they only focus on one-dimensional motion. However in many robotic manipulation applications the objects move on a plane e.g. when an object can move in the robotic gripper depending on the grasping force. One-dimensional models cannot capture these multi-dimensional motions like sliding and spinning. Therefore it is necessary to model friction not only for a one-dimensional motion but also for planar motion. There are models that combine translational and rotational friction, but only the Coulomb friction model has been taken into account. Thus in this thesis the combination of different friction models and planar motion is examined. To achieve this the computation of the states of the more refined friction models were changed to include constraints that arise for multi-dimensional friction modelling. These constraints allow the coupling of translational and rotational motion as the frictional forces for both motions are interacting.

Acknowledgements

First I would like to express my sincere gratitude to my thesis advisor Mr. Yiannis Karayiannidis, an Assistant Professor at Chalmers University of Technology, for his continuous support of my thesis project. His constructive comments and suggestions were a great help to me.
I also would like to thank Mr. Michael Seyfarth for the uncomplicated supervision on the part of the University of Stuttgart.

Contents

List of Figures

List of Tables

Notation

Symbols

Symbol	Unit	Description
A	m^2	Contact area
$\boldsymbol{A}$	-	Frictional matrix
c	m	Distance between centre of rotation and origin of coordinate system
$\boldsymbol{e_v}$	-	Unit vector of translational velocity
$\boldsymbol{e_\omega}$	-	Unit vector of rotational velocity
E	-	Complete elliptic integral of the second kind
$f_{applied}$	N	Force applied on a body
f_C	N	Coulomb friction constant
f_f	N	Friction force
f_{max}	N	Maximal static friction level
f_n	N	Normal force
f_r	N	Resultant tangential force
f_{ss}	N	Stribeck force
f_x	N	Friction force along x-axis
f_y	N	Friction force along y-axis
g	$^{m}/_{s^2}$	Gravitational acceleration
I	m^2kg	Moment of inertia
k	$^{N}/_{m}$	Stiffness of spring
K	-	Complete elliptic integral of the first kind
m	kg	Point mass of the object
M	Nm	Torque
m_z	Nm	Friction torque normal to z-axis
$\boldsymbol{r}$	-	Vector describing the position of an infinitesimal small area
$\boldsymbol{r_0}$	-	Vector from the origin of the coordinate system to a local area

Symbol	Unit	Description
R	m	Radius of a disk
s	m	Rigid body displacement of the object
p	$^{\mathrm{N}}/_{\mathrm{m}^2}$	Pressure
v	-	Absolute value of translational velocity
$\boldsymbol{v}$	-	Vector of translational velocities
w	m	Plastic (irreversible) component of body displacement
x	m	Total body displacement
$\dot{x}$	$^{\mathrm{m}}/_{\mathrm{s}}$	Translational velocity of the object
$\dot{x}_s$	$^{\mathrm{m}}/_{\mathrm{s}}$	Critical velocity for Stribeck effect
δy	m	Microscopic translational displacements
z	m	Elastic (reversible) component of body displacement
z_{ba}	m	Breakaway displacement
z_{ss}	m	Steady-state deflection
α	-	Parameter for Elasto-Plastic Model
γ	-	Ratio of microscopic displacements
ϵ	-	Ratio of translational and rotational velocity
μ_d	-	Independent coefficient of dynamic friction
μ_s	-	Independent coefficient of static friction
σ_0	$^{\mathrm{N}}/_{\mathrm{m}}$	Contact stiffness
σ_1	$^{\mathrm{Ns}}/_{\mathrm{m}}$	Damping for tangential compliance
σ_2	$^{\mathrm{Ns}}/_{\mathrm{m}}$	Viscous friction parameter
τ_f	Nm	Frictional torque
$\delta\varphi$	-	Microscopic Rotation
ω	$^{1}/_{\mathrm{m}}$	Absolute value of rotational velocity
$\boldsymbol{\omega}$	-	Vector of rotational velocity

Chapter 1

Introduction and Related Work

1.1 Context

Robots have been used in many different production systems in industry. Industrial robots work in known environments and their tasks are defined clearly. If the movement of robots and forces needed to be assigned in order to perform a task are known, it is possible to derive the control effort off-line. In case of industrial robots, one of the main sources of uncertainties is friction in the joints. To deal with uncertainties in friction in the robot joint, much research has been done to model friction.
However, in recent years there is an increase in the usage of robots not only in many different industrial areas but also in human-centred environments. For example in industrial environments, more recent concepts of object manipulation tasks include in-hand manipulation and pushing an object across a flat surface. Due to new applications resulting from this broader scope of usage, new issues arise. One of these new applications is object manipulation done by robots with simple grippers. To do manipulation tasks efficiently, it is necessary to understand many physical processes. For example, one process is the friction between the robot and the object that should be manipulated. It is necessary to know the force needed to manipulate the object as precisely as possible because the object must not be damaged by the robot and it should be done efficiently. An example of efficient object manipulation is to push the object so that it slides on a surface. To do such tasks it is necessary to compute the force needed in real time which in turn requires accurate friction models. In the past many models were developed that change their structure when friction changes from static to dynamic or in reverse. In such models it can be necessary to reinitialise the simulation with a different model. To avoid this, different approaches without a structural change are

needed.

1.2 Definition of Topic

The purpose of this project is to gain a thorough understanding of friction modelling with a focus on friction models applicable to object manipulation. This aim requires understanding of different friction phenomena with a focus on friction at low velocities. As it is aimed to develop a general friction model applicable to a wider range of scenarios, it should allow to include planar motions.
Thus, the developed model has to result in a continuous friction force without change of model when transitioning between static and dynamic friction. Furthermore, the model should predict friction both accurately and efficiently to be usable in robotic manipulation. For an efficient use it is also essential to identify the conditions the model is valid for.

1.3 Related Work

Friction is an ongoing research topic from the times of Leonardo da Vinci [2] until today. Nowadays for example, friction models are part of simulations used to predict behaviour in object manipulation [3]. To do efficient object manipulation tasks with simple grippers, it is necessary to allow external forces like gravity to act on the object and control the sliding motion of the object [4]. Additionally to grasping, it is possible to move objects by pushing them across a surface. For both applications it is essential to understand the principles of friction to readjust correctly the grasp and forces needed as described in [4].
Furthermore, an accurate model is needed to predict operating point stability and performance, see [5]. Such accurate models are also important when small motions are simulated. Therefore, it is important to predict correctly whether the object moves or stays in the same place. However, friction properties depend on the movement of the object. In [6] it is described that there is an interplay of transitional and rotational movement that affects sliding. This connection was shown by independent research groups, for example in [7] and [8]. One such result is that in the case of a spinning and sliding disk both translational and rotational movement stop at exactly the same time [9].
While Dahmen et al. consider the onset of sliding with both transitional and rotational movement in [6], a different research project pays close attention

to slowing down movement [7].
As described in [2], in the case of static friction the maximal friction force is a product of the normal force and a coefficient. In the case of dynamic friction, the friction force is a product of the normal force and a kinetic coefficient that is usually smaller than the coefficient in the static case. Additionally, a further term can be added to describe the viscous friction. This friction phenomenon is proportional to the velocity.
Other models (described in [3]) do not need different structures in the case of static or dynamic friction. One example of such a model was published by Dahl in 1968 [10]. As Dahl's model excludes friction phenomena that are linked to the case of lubricated friction, a generalised model known as LuGre Model [5] was developed. The model's name originates from the two cities it was developed in: Lund and Grenoble [11]. However both Dahl's model and the LuGre model exhibit drift instead of static friction, see [3].
Other friction phenomena that have to be taken into account are described in [5]. For example the dominant friction phenomenon in high-precision pointing can be presliding, that is the transition between static and dynamic friction. As shown in [6], the microscopic process during presliding is still not fully understood.
To sum up, there are various friction models that are useful for different one-dimensional applications. However, existing planar motion models are based on the Coulomb friction model. Therefore, this thesis seeks to examine the possibilities of simulating planar motion using other friction models.

1.4 Approach and Scope of the Thesis

In this thesis, general friction models will be developed after gaining understanding of physical principles involved in friction phenomena. These models should not change their structures under transition between different friction phenomena. To guarantee a smooth modelling of applications, it is necessary to be aware of critical points within the model that result in limitations of the usage of the model. Regarding a general friction model, it is important to know what material characteristics and forces, such as the applied force and gravity, need to be taken into account to allow a more precise modelling. To evaluate the usability of a model, each model will be compared to others that evolved based on different theoretical approaches, either the aim of the model is to mimic experimental data or it resembles certain physical phenomena most closely. When modelling friction, a clear understanding of the model properties is needed to determine what friction phenomena are described in the particular model. Since different amounts of friction phe-

nomena are covered in the models, the applicability of models vary. These restrictions will be taken into account when developing a general model.
As the models are chosen with manipulation tasks in mind, there is no focus on friction in combination with lubricated surfaces. Furthermore, special consideration will be placed on models that predict friction with low forces and low velocities. Additionally, the models should include not only translational movement but planar motion so that it is possible to predict reach and direction of sliding motion. For this, friction models for rotational and translational movement need to be coupled.
Following the models' generation, the models will be applied to specific applications for testing purposes without fine-tuning. This will be done to gauge the model's usefulness in practical applications. After testing, it will be evaluated if there is a model most fitting for general usage.
This thesis begins with a theoretical review of different friction models and friction phenomena in chapter 2. In the next two sections, there are introductions of planar friction modelling and their application to both the Coulomb and the elasto-plastic friction model. These different models are compared in chapter 5 when they are applied to exemplary test cases.

Chapter 2

Comparison of Friction Models

In the past, many different friction models were developed. To allow for a comparison of friction models, all models are described to be used in the following minimal working example: An external force $f_{applied}$ is applied to an

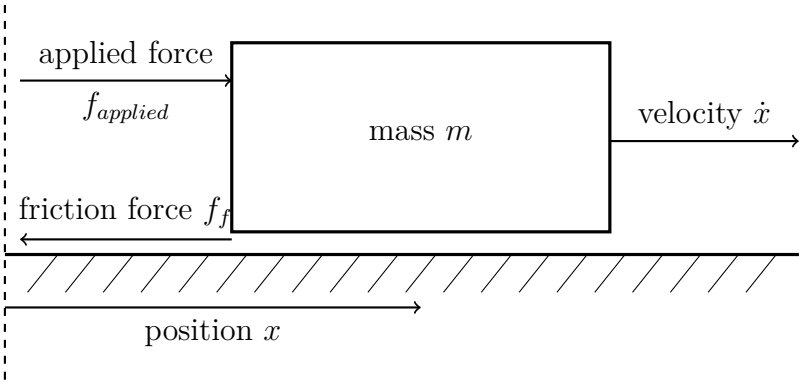

Figure 2.1: Body moving under the influence of friction and externally applied force.

object with mass m at is at position x as shown in figure 2.1. In this scenario, a reacting force is the frictional force f_f. In the case of dynamic friction, the objects moves with the velocity $\dot{x}$. There are many different attempts to model this translational friction f_f. However, to stay close to common descriptions of the friction models, all friction forces but the Coulomb friction force (section 2.1) are defined in the opposite direction.

2.1 Coulomb Model

One of these models is the Coulomb friction model. This model includes stiction and kinetic friction. Stiction is the static friction that arises when the applied force is not large enough to overcome the threshold necessary to slide. When the applied force is bigger than the threshold, the object starts sliding. Then the applicable friction phenomenon is kinetic friction. For a one-dimensional case, both static and kinectic friction can be described by the following equation:

$$f_f \leq -\mu_d f_n \cdot \text{sign}(\dot{x}) \tag{2.1}$$

where f_f is the resulting friction force, μ_d a dimensionless parameter describing the coefficient of friction, f_n the resulting normal force, and $\dot{x}$ the velocity of the object. The parameter μ_d depends on the materials used but not on the velocity or the normal force f_n [4]. The cases of static and dynamic friction can be distinguished by the inequality. In the case of static friction the inequality applies as the normal force is not enough to initiate a movement. However, in the dynamic case the equality describes the resulting friction force f_f[4]. The resulting friction force f_f always is opposed to the direction of the resulting movement. As seen in figure 2.3 equation (2.1) leads to a constant friction force under the assumption of a constant normal force. This friction force is called the Coulomb friction constant f_C [12]:

$$f_C = \mu_d f_n \tag{2.2}$$

In equation (2.1) only the normal component of the applied force is considered. However, the applied force is not limited to this direction. It can be seen in figure 2.2 that the normal component of the applied force can be computed using geometric principles. In this example the resulting normal force is defined by:

$$f_n = f_{applied} \cdot \sin(\beta) + m \cdot g \tag{2.3}$$

where g is the gravitational acceleration.

Furthermore, the magnitude of the frictional force is independent of the velocity of the object. This relation can be seen in figure 2.3.

2.2 Enhancements of the Coulomb Model

The model described in section 2.1 is often used because of its simplicity [13]. However, the Coulomb model does not predict friction accurately enough as many phenomena are ignored. Viscous friction is one of these phenomena.

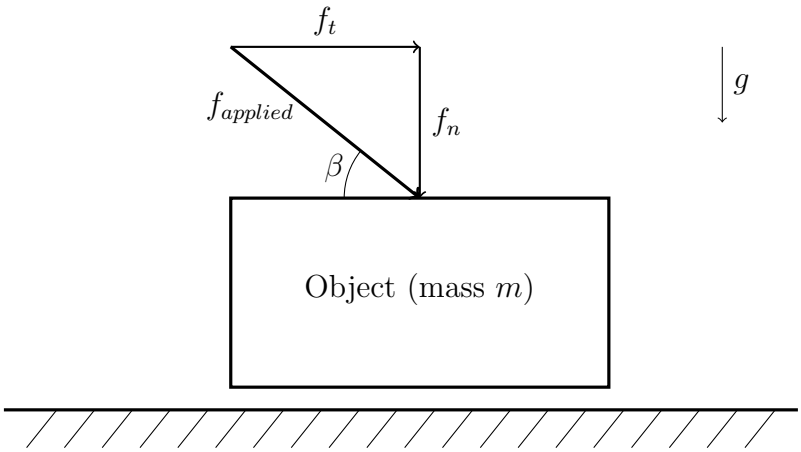

Figure 2.2: External force from an arbitrary direction acting on a body.

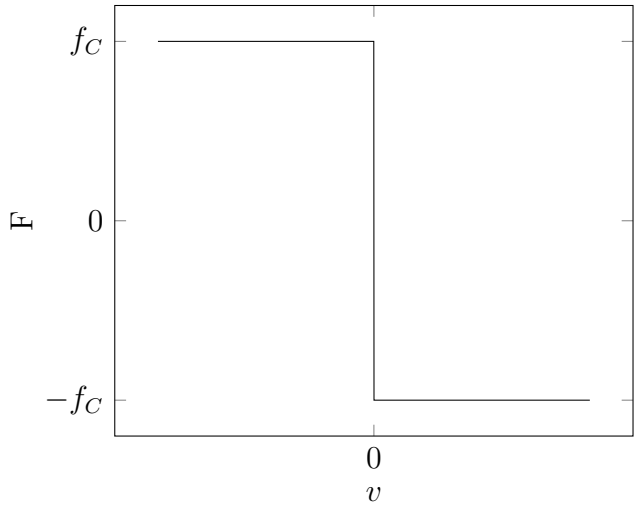

Figure 2.3: Friction force modelled with Coulomb model.

In the case of viscous friction the moving object and the surface below are separated by a lubrication layer. This viscous friction depends proportionally on velocity. Because of this proportionality, the influence of viscous friction is zero when the object does not move [14].
To include this phenomenon the model described above was extended as follows [13]:

$$f_f = \begin{cases} f_f(\dot{x}) & \text{if } \dot{x} \neq 0 \\ f_r & \text{if } \dot{x} = 0 \text{ and } |f_r| < f_C \\ f_C \cdot \text{sign}(f_r) & \text{if } \dot{x} = 0 \text{ and } |f_r| \geq f_C \end{cases} \tag{2.4}$$

where f_r is a resultant tangential force, and f_C the Coulomb friction constant. In the case of zero velocity the possible friction force is limited by the Coulomb friction constant f_C. As long as the force is below this threshold, the friction force is equal to the resultant tangential force f_r.
If the force is larger that this threshold, the body can start to slide. In this case the resultant friction force depends on the velocity of the body. By considering a simple viscous friction model where viscous friction is proportional to the velocity, the friction force f_f of (2.4) can be written as follows [2]:

$$f_f(\dot{x}) = f_C \text{sign}(\dot{x}) + \sigma_2 \dot{x} \tag{2.5}$$

where σ_2 is the viscous friction constant. The friction force is shown in figure 2.4.

In experiments the following was discovered: If the friction force increases continuously then the velocity increases. However, at low velocities the frictional force first decreases before it increases again. This behaviour can be seen in figure 2.5. As this phenomenon was first observed by Stribeck, it is called Stribeck friction or Stribeck effect. To include the Stribeck effect, equation (2.5) has been modified as follows [15]:

$$f_f(\dot{x}) = f_C \cdot \text{sign}(\dot{x}) + (f_{max} - f_C) e^{-|\frac{\dot{x}}{\dot{x}_s}|^2} + \sigma_2 \dot{x} \tag{2.6}$$

where $\dot{x}_s$ is the Stribeck velocity and f_{max} the maximal static friction force:

$$f_{max} = \mu_s f_n \tag{2.7}$$

where μ_s is the static coefficient of friction analogous to μ_d in the dynamic case. Therefore f_{max} is the static equivalent to the Coulomb friction coefficient f_C as defined in (2.2). In general, it holds that:

$$\mu_s \geq \mu_d \tag{2.8}$$

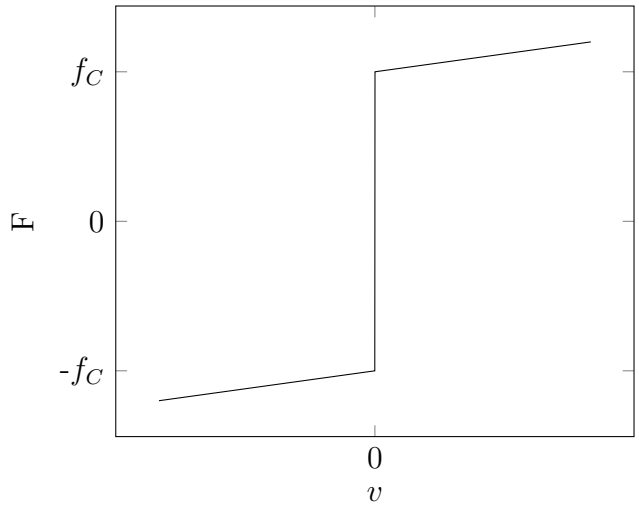

Figure 2.4: Friction force modelled by enhanced Coulomb model to include viscous friction.

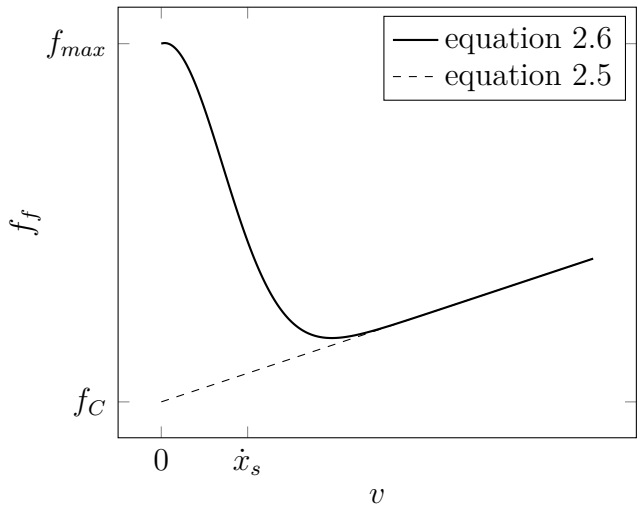

Figure 2.5: Stribeck effect included in the friction force modelling.

The Stribeck velocity $\dot{x}_s$ describes the characteristic velocity at which the friction changes between the static and kinetic friction [15]. This parameter determines how fast the friction force f_f converges to the Coulomb friction constant [16]. As seen in figure 2.5 accounting for the Stribeck effect results in a smooth friction force [3]. The parameters needed for this parametrisation can be evaluated experimentally [13].

2.3 Dahl's Model

In 1968, Philip R. Dahl published a different friction model [10]. This model was developed to fit experimental data better and in order to be able to model presliding in control applications [5].
Presliding is a friction phenomenon that describes the motion before the object slips completely [5]. Because of this, it describes the transition between static and kinetic friction. This phenomenon occurs during the transition, because at asperity contacts the adhesive forces dominate the frictional behaviour. Compared to other friction phenomena it is a function of displacement rather than velocity [17]. In this model the friction force f_f monotonically approaches the Coulomb friction constant f_C. If the velocity $\dot{x}$ is positive f_f will tend to $+f_C$, if $\dot{x}$ is negative it will approach $-f_C$ [18].

$$\frac{df_f(x)}{dt} = \sigma_0 \left| 1 - \frac{f_f}{f_C} \cdot \text{sign}(\dot{x}) \right|^i \text{sign}\left(1 - \frac{f_f}{f_C} \cdot \text{sign}(\dot{x}) \right) \tag{2.9}$$

In this model the friction force is depended on the contact stiffness σ_0 as well as on the exponent i. This parameter i describes the friction law used and changes the model for different material characteristics. In the case of ductile materials the exponent should be $i = 1, 2$ and for brittle materials $i = 0, 0.25, 0.5$ [18]. However, the value $i = 1$ is used typically [5].
Because of comparability, the representation of Dahl's model in [5] will be used and can be seen in figure 2.6:

$$f_f = \sigma_0 z, \quad \sigma_0 > 0, \quad \dot{z} = \dot{x} \left(1 - \frac{\sigma_0}{f_C} \cdot \text{sign}(\dot{x}) z \right)^i \tag{2.10}$$

where x is the body displacement and z the elastic component of the displacement.
Compared to the previous models, the Dahl's model can be used to predict presliding displacement with the single continuous state z [5]. An advantage of this model is, that the resulting friction force is smooth even when the velocity crosses zero and therefore avoids discontinuity [3]. However, under

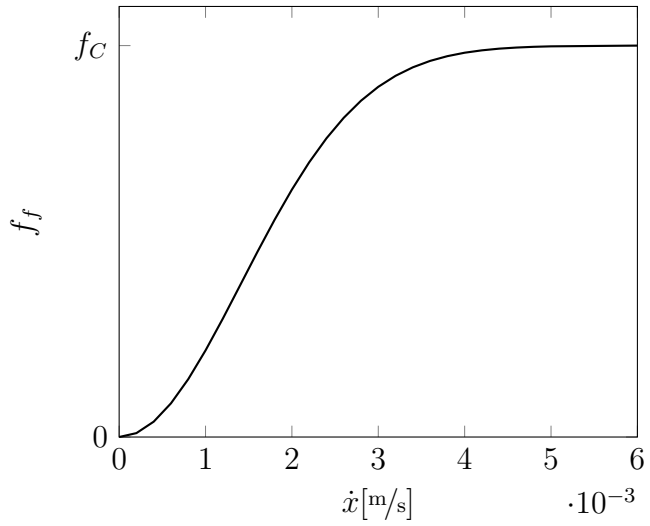

Figure 2.6: Friction force depended on velocity modelled with Dahl's model.

certain circumstances simulations using this model can show drift instead of static behaviour [3] as Dahl's model does not capture static friction [13]. Furthermore, Dahl's model is not able to model the Stribeck effect [12].

2.4 LuGre-Model

In order to include the viscous friction phenomenon, the model of the friction force described in (2.10) was modified as follows:

$$f_f = \sigma_0 z(t) + \sigma_1 \dot{z}(t) + \sigma_2 \dot{x}(t) \tag{2.11}$$

where σ_1 is the parameter that is used to damp tangential oscillations of the elastic displacement [3] and parameter σ_2 describes the influence of viscous friction. Combining this parameter with the elastic displacement results in a frictional memory in the case of slipping. Because of the parameter σ_1 the LuGre-Model is able to model stiction, as the elastic displacement takes place before sliding. After the onset of sliding, the term $\sigma_1 \dot{z}(t)$ loses its importance [16]. Thus, an accurate value of σ_1 is important to model systems that predict slow movements.
In the following for clarity of presentation the argument of time t will be omitted. The state z is governed by:

$$\dot{z} = \left(1 - \frac{z}{z_{ss}(\dot{x})}\right) \dot{x} \tag{2.12}$$

where z_{ss} is the steady-state deflection. This deflection can be computed with the help of the steady-state friction force f_{ss} that is defined later in the text using the following relation:

$$z_{ss} = \begin{cases} \frac{f_{ss}(\dot{x}(t))}{\sigma_0} & |\dot{x}| > 0 \\ \frac{f_{max}}{\sigma_0} & \dot{x} = 0 \end{cases} \tag{2.13}$$

Both branches for deflection include the normal force f_n in the friction models.
The two cases in (2.13) are needed to insure that z_{ss} is defined in the case of zero velocity [3]. This steady-state friction force is also called the Stribeck curve and can be modelled in various ways [3]. One such equation reads as follows:

$$f_{ss}(\dot{x}) = \left[(f_{max} - f_C)e^{-(\dot{x}/\dot{x}_s)^2} + f_C\right] \text{sign}(\dot{x}) \tag{2.14}$$

A different variant to compute f_{ss} is:

$$f_{ss}(\dot{x}) = \left[(f_{max} - f_C)\frac{1}{1 + (\frac{\dot{x}}{\dot{x}_s})^2} + f_C\right] \text{sign}(\dot{x}) \tag{2.15}$$

As shown in figure 2.7 both forms show a similar behaviour. However, equation (2.15) is more efficient for computational purposes [3].
By introducing the Stribeck curve in the friction model, the Stribeck effect described in 2.2 can be modelled. This is important for friction modelling at low velocities as it allows to distinguish more accurately between stick and slip. In the case of stiction, the friction force is smaller than the steady-state friction force. Therefore the object has zero velocity although an external force is applied. A motion that alternates between stick and slip at low velocities is called a ”stick-slip motion”.

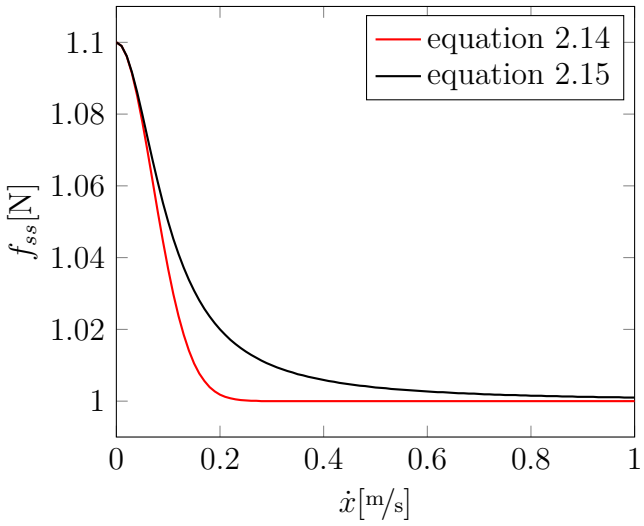

Figure 2.7: Graph of different forms for computing f_{ss} using $f_{max} = 1.1\,\mathrm{N}$, $f_C = 1\,\mathrm{N}$ and $\dot{x}_s = 0.1\,\mathrm{m/s}$.

2.5 Elasto-Plastic Model

A further advancement of the friction models that use an additional state is the so-called elasto-plastic model. The conceptual idea of the elasto-plastic model is to include microscopic reversible displacements that occur as the material experiences stress. When a force is applied to an object, asperity contacts of the material deform as seen in figure 2.8. If the stress is low enough, the movement of asperity contacts will be reversed without movement of the object. This reversible displacement z is called elastic motion. Once the object begins sliding, it moves irreversible (called "plastic" displacement); it is associated with the notation w. In order to include both irreversible plastic and reversible elastic displacement, the total displacement x is defined as the sum of both components: $x = z + w$.

The used friction force is the same as for the LuGre model, described in equation (2.11). However the state z is governed by:

$$\dot{z} = \left(1 - \alpha(z, \dot{x})\frac{z}{z_{ss}(\dot{x})}\right)\dot{x}(t) \tag{2.16}$$

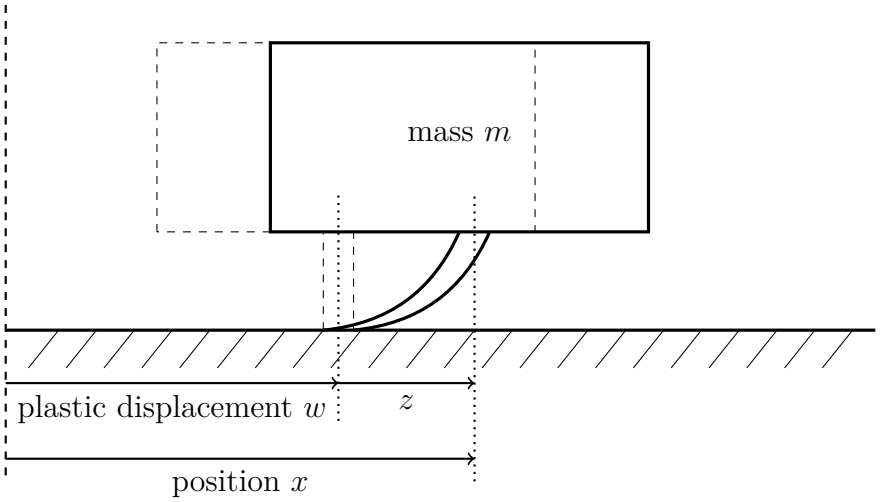

Figure 2.8: Elastic and plastic displacement of an object based on asperity contacts.

where α is a piece-wise defined function that controls the rate of change of the state z:

$$\alpha(z,\dot{x}) = \begin{cases} 0 & |z| \leq z_{ba} \\ \frac{1}{2}\sin\left(\pi \frac{z-\left(\frac{z_{ss}+z_{ba}}{2}\right)}{z_{ss}-z_{ba}}\right) & z_{ba} < |z| < z_{ss}(\dot{x}) \\ 1 & |z| \geq z_{ss}(\dot{x}) \end{cases} \tag{2.17}$$

where z_{ba} is the breakaway displacement that allows for stiction as the model shows elastic behaviour for $|z| < z_{ba}$ [19]. This breakaway displacement is necessary to allow for small elastic motions that do not lead to sliding even if it is accumulated [3]. For the object to start sliding, the friction force has to become larger than the associated breakaway force.
Since the Stribeck curve is used, the elasto-platic model can predict Stribeck effect like the LuGre model. The elasto-plastic model includes all friction phenomena that are also included in the LuGre-model but it also includes stiction [19].
When both directions of the velocity $\dot{x}$ and of z are the same, then α is a piece-wise continuous function. This case is plotted in figure 2.9. If the directions of $\dot{x}$ and z differ, α will be defined to be zero [3]. The state of the irreversible displacement w is governed by [3]:

$$\dot{w} = \alpha(z,\dot{x})\frac{z(t)}{z_{ss}(t)}\dot{x}(t) \tag{2.18}$$

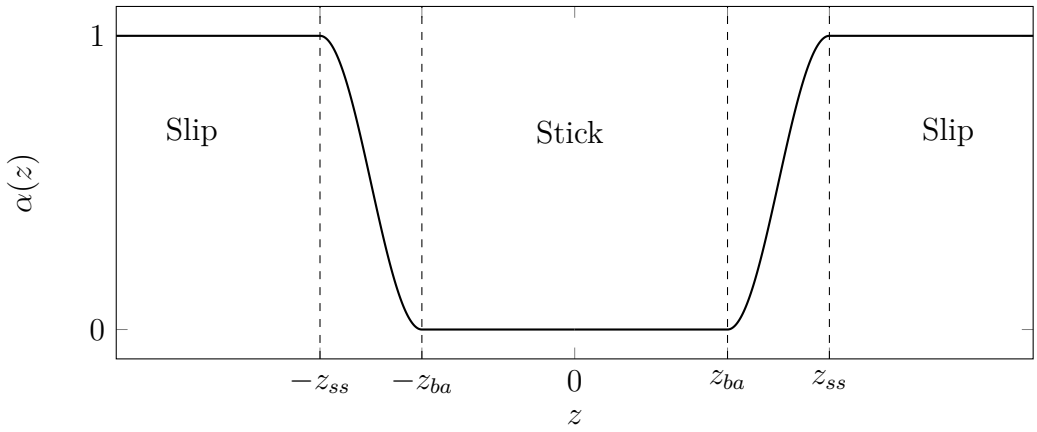

Figure 2.9: Plot of parameter α if $\text{sign}(\dot{x}) = \text{sign}(z)$

In the elasto-plastic model the stick-slip behaviour is defined as follows: In the case of sticking, only elastic displacement occurs. Therefore it holds that:

$$\dot{x} = \dot{z} \qquad \dot{w} = 0 \tag{2.19}$$

However, in the case of sliding only the plastic displacement is relevant:

$$\dot{x} = \dot{w} \qquad \dot{z} = 0 \tag{2.20}$$

In comparison, the LuGre model does not differentiate between elastic and plastic movement since only the dynamics of the elastic motion are taken into account. The additional distinction between LuGre and elasto-plastic model is the modelling of the stick-slip effect. While the LuGre model includes the stick-slip effect, the transition between stick and slip is not modelled explicitly as is done with the parameter α in the elasto-plastic model. When only elastic motion occurs as shown in equation (2.19), the dynamics of the LuGre model and the elasto-plastic model are identical if it holds that $\alpha = 1$.

2.6 Summary of models

In the following there is a summary of the presented friction models. The table 2.1 includes both the captured friction phenomena and the needed parameters.

Table 2.1: Summary of presented friction models.

Model	Parameters	State variable	Stiction	Viscous friction	Stribeck	Presliding	Stick-Slip
Coulomb	f_n, μ_d		Yes	No	No	No	No
Enhanced Coulomb 2.5	f_n, μ_d, σ_2		Yes	Yes	No	No	No
Enhanced Coulomb 2.6	f_n, μ_d, μ_s, σ_2, $\dot{x}_s$		Yes	Yes	Yes	No	No
Dahl	f_n, μ_d, σ_0, i	z	No	No	No	Yes	No
LuGre	f_n, μ_d, μ_s, $\dot{x}_s$, σ_0, σ_1, σ_2	z	Yes	Yes	Yes	Yes	Yes
Elasto-Plastic	f_n, μ_d, μ_s, $\dot{x}_s$, σ_0, σ_1, σ_2, z_{ba}	z	Yes	Yes	Yes	Yes	Yes

Chapter 3

Friction Models for Planar Motion: Sliding and Spinning

In chapter 2, it is only considered that an object moves one-directional, for example translationally. However, that is a strong restriction. In this chapter, movements in more directions will be discussed.
These models will simulate the behaviour of a disk with radius R and mass m that slides and spins on a flat surface. Like it is shown in figure 3.1 the disk slides with the translational velocity v and spins with the angular velocity ω. This results in both a frictional force f_f as well as a frictional torque τ_f.

In the case of multi-dimensional friction behaviour a modification of the translational friction models is necessary since experiments show that an object slides further when it is spinning at the same time compared to an object that only slides [7]. Because of this, it is clear that less force is needed to move an object that is spinning and sliding simultaneously. A further reason for enhancing translational friction models can be shown for purely sliding objects. Consider an object that moves in a Cartesian coordinate system. However, it does not move along an axis. When only translational friction models are taken into account to model the frictional behaviour of this object, it would be possible to model friction with the help of two independent models along both axis. In one-dimensional friction models the friction force is bounded, for example in Coulomb's model by the Coulomb friction constant f_C. As shown in figure 3.2 it is possible for two independent friction forces that simulate the frictional behaviour of a single object to become larger than the boundary force f_C. To prevent this occurrence friction models for multiple dimensions have to be coupled.

In planar motion it is important to consider the microscopical process that happens when links between the object and the surface break.
In literature two scenarios are discussed.

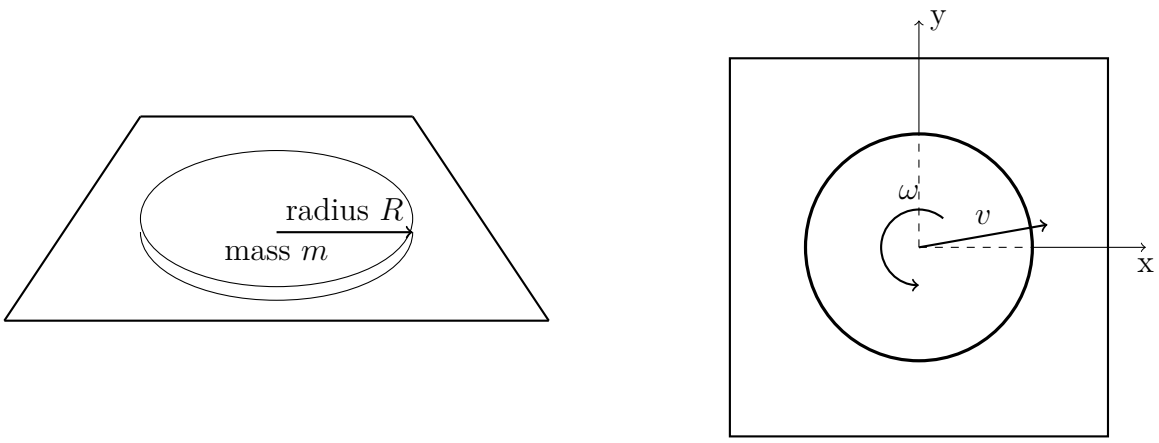

Figure 3.1: Schematic view of a sliding and spinning disk.

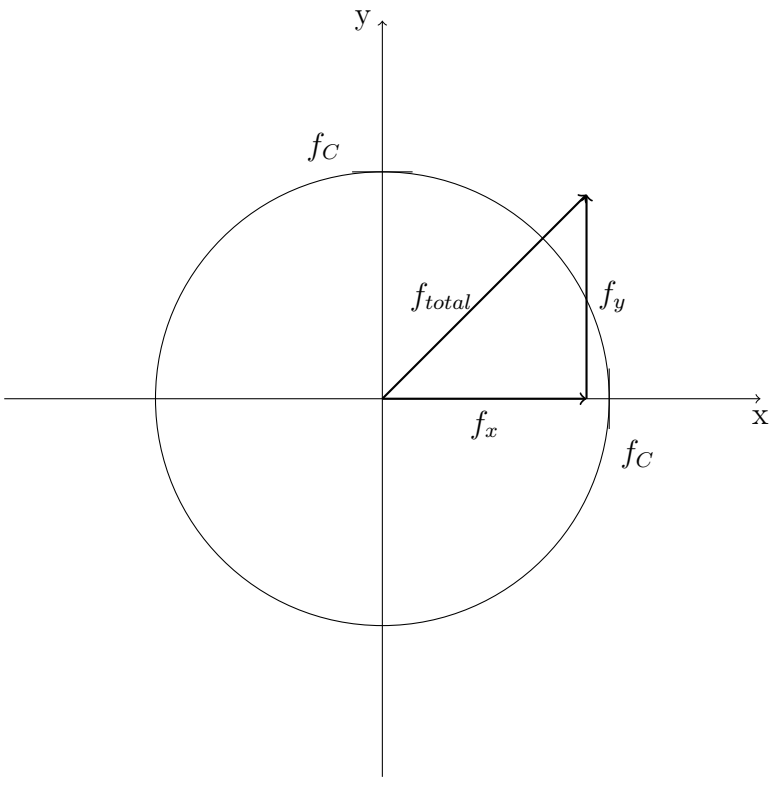

Figure 3.2: Friction force in x direction f_x and in y direction f_y add to a friction force f_{total} larger than f_C.

1. In the first theory it is assumed that each microscopical link experiences its own set of force and torque. Therefore the links break at individual times. Furthermore, it is assumed that the links do not reestablish themselves after their breaking. Thus, the applied force and torque on the whole object distribute on fewer links resulting in higher forces and torques for each link. Therefore the breaking of links happens like an avalanche [6]. In [6] it is shown that the friction force and torque are proportional in this scenario.

2. The second scenario differs from the first in the assumption that broken links reestablish themselves immediately after the breaking. This breaking and reestablishing of links happens until all links experience approximately the same stress. Because of this, all links break finally at the same time when the object begins moving [6]. For this case the theoretical relation between frictional force and torque is non-linear [6].

3.1 Friction Models for Rotational Movement

In this section a multi-dimensional friction theory is presented. This theory is based on the Coulomb friction model as described in equation (2.1). To allow for more diverse external forces instead of the normal force f_n, a pressure distribution is used. The pressure distribution $p(x, y)$ describes the local pressure on an infinitesimal area at position (x, y). Therefore the normal force f_n at position (x, y) can be computed as:

$$\frac{df_n}{dA} = p \tag{3.1}$$

where dA is the infinitesimal large area [4].
As the friction force in equation (2.1) is independent of the velocity but the direction of movement is important, instead of using $\text{sign}(\dot{x})$ the unit vector will be used $\frac{\boldsymbol{v}(x,y)}{|\boldsymbol{v}(x,y)|}$ where $\boldsymbol{v}(x, y)$ is the translational velocity of the body.
A further change compared to the Coulomb model is to allow different friction coefficients. Thus the constant μ_d changes to reflect the specific friction coefficient for an infinitesimal area: $\mu_d(x, y)$.
In order to be able to compute friction force and torques the following conditions should be met [4]:

- The body is sliding on a planar surface.
- The pressure distribution across the contact area between body and surface $p(x, y)$ is known.

- The friction coefficient $\mu_d(x, y)$ is known.

With these assumptions the general friction force according to [4] is:

$$f_f = -\int_{\text{contact area}} \mu_d(x,y)p(x,y)\frac{\boldsymbol{v}(x,y)}{|\boldsymbol{v}(x,y)|}dA \tag{3.2}$$

Under the same conditions the associated frictional torque m_f is:

$$\tau_f = -\int_{\text{contact area}} \mu_d(x,y)p(x,y)\left[\boldsymbol{r_0} \times \frac{\boldsymbol{v}(x,y)}{|\boldsymbol{v}(x,y)|}\right]dA \tag{3.3}$$

where $\boldsymbol{r_0}$ is the vector from the origin of the coordinate system to the local area where friction is computed and the symbol $\times$ signifies the cross-product. As equations (3.2) and (3.3) depend both on the specific local pressure distribution $p(x, y)$ and coefficient of friction $\mu_d(x, y)$ the integral cannot be solved in general. Analytic solutions only exist for few special cases [4].
However, it is possible to simplify these equations for the case of axisymmetric pressure distribution and axisymmetric contacts. Under this assumption and the help of transformation of coordinate systems equations (3.2) and (3.3) can be rewritten in polar coordinates (r, θ) as follows:

$$f_f = -\int_0^{2\pi}\int_0^R \mu_d(r)p(r)\frac{(r\cos\theta - c)r}{\sqrt{r^2 + c^2 - 2rc\cos\theta}}drd\theta \tag{3.4}$$

$$\tau_f = -\int_0^{2\pi}\int_0^R \mu_d(r)p(r)\frac{(r - c\cos\theta)r^2}{\sqrt{r^2 + c^2 - 2rc\cos\theta}}drd\theta \tag{3.5}$$

where c describes the distance between the origin of the coordinate system and the current centre of rotation and R is the radius of the contact area.
Even with the reduction to axisymmetric pressure distribution and contacts, analytic solutions only exist for special cases. The equations (3.4) and (3.5) are elliptic integrals. This can be used to solve special cases.
One such special case is the sliding and spinning of a homogeneous flat disk with a constant pressure distribution. Therefore, the pressure distribution can be represented as the ratio of the formal force f_n that acts on the complete area of the disk and the corresponding area:

$$p = \frac{f_n}{\pi \cdot R^2} \tag{3.6}$$

Furthermore, the friction coefficient is assumed to be constant μ. With this assumptions the Coulomb friction can be written for multiple dimensions as:

$$\boldsymbol{f_f} = -\frac{\mu_d f_n}{\pi R^2}\int_{\text{contact area}} \frac{\boldsymbol{v} + \boldsymbol{\omega} \times \boldsymbol{r}}{|\boldsymbol{v} + \boldsymbol{\omega} \times \boldsymbol{r}|}d^2r \tag{3.7}$$

where $\boldsymbol{\omega}$ describes the angular velocity of the disk [7]. Similarly, the friction torque can be written as:

$$\boldsymbol{\tau_f} = -\frac{\mu_d f_n}{\pi R^2} \int_{\text{contact area}} \boldsymbol{r} \times \frac{\boldsymbol{v} + \boldsymbol{\omega} \times \boldsymbol{r}}{|\boldsymbol{v} + \boldsymbol{\omega} \times \boldsymbol{r}|} d^2 r \tag{3.8}$$

In [7] it is stated that the friction force and torque depend only on the dimensionless ratio

$$\epsilon = \frac{v}{R \cdot \omega} \tag{3.9}$$

where v is the absolute value of $\boldsymbol{v}$ and ω is the absolute value of $\boldsymbol{\omega}$. Furthermore, the friction force does only depend on the direction of the relative velocity. Therefore Farkas et al. present the analytical solution of equation (3.7) for a flat disk [7]:

$$\boldsymbol{f_f} = -\mu_d f_n \boldsymbol{e}_v \mathcal{F}(\epsilon) \tag{3.10}$$

where $\boldsymbol{e}_v$ is the normalized translational velocity and $\mathcal{F}(\epsilon)$ is defined as follows:

$$\mathcal{F}(\epsilon) = \begin{cases} \frac{4}{3} \frac{(\epsilon^2+1)E(\epsilon^2)+(\epsilon^2-1)K(\epsilon^2)}{\epsilon\pi} & \epsilon \leq 1 \\ \frac{4}{3} \frac{(\epsilon^2+1)E(\frac{1}{\epsilon^2})-(\epsilon^2-1)K(\frac{1}{\epsilon^2})}{\pi} & \epsilon \geq 1 \end{cases} \tag{3.11}$$

where $K(\epsilon)$ and $E(\epsilon)$ are the first and the second kind of complete elliptic integrals. It is important to note that in this thesis the inputs for the complete elliptic integrals are in squared form.
The friction torque is presented accordingly to be:

$$\boldsymbol{\tau_f} = -\mu_d f_n R \boldsymbol{e}_\omega \mathcal{T}(\epsilon) \tag{3.12}$$

where $\boldsymbol{e}_\omega$ is the normalized angular velocity and $\mathcal{T}(\epsilon)$ is given by:

$$\mathcal{T}(\epsilon) = \begin{cases} \frac{4}{9} \frac{(4-2\epsilon^2)E(\epsilon^2)+(\epsilon^2-1)K(\epsilon)}{\pi} & \epsilon \leq 1 \\ \frac{4\epsilon}{9} \frac{(4-2\epsilon^2)E(\frac{1}{\epsilon^2})+(2\epsilon^2-5+\frac{3}{\epsilon^2})K(\frac{1}{\epsilon^2})}{\pi} & \epsilon \geq 1 \end{cases} \tag{3.13}$$

The analytical solutions described here were first published in [7] and later corrected in [6].
Both equations (3.11) and (3.13) result in smooth lines as both the equations and their derivatives are identical for the left-hand and right-hand sides. These curves are shown in figure 3.3.

The connection of friction force and torque is shown in figure 3.4 and was discovered by various research groups. This curve lies in accordance with the second scenario mentioned in section 3. That means that the micro-contacts between the object and the surface immediately reestablish themselves after

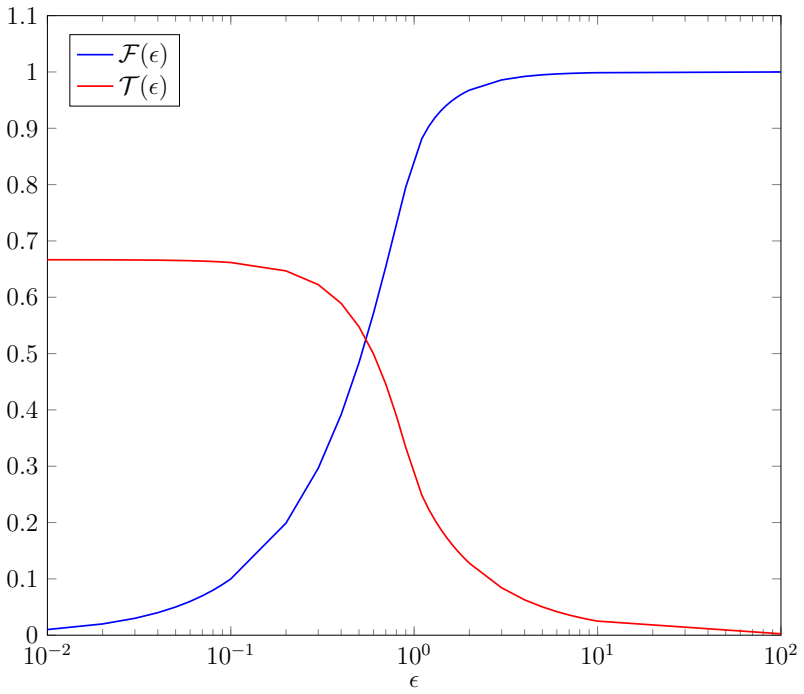

Figure 3.3: Plot of the dimensionless friction force $\mathcal{F}$ and $\mathcal{T}$ over the ratio ϵ.

breaking until all links experience nearly the same stress [6].
Figure 3.4 shows the elliptic curve that displays the critical point for each pairing of force and torque. If the force and torque combination is below the curve, the object will not start moving. However, with a combination above the curve the object moves. If the object is already moving and any combination above the curve is applied, the object will accelerate [20].

3.2 Modelling the onset of sliding

To model the onset of sliding accurately, it is important to be able to determine the force and torque combination that will lead to movement. However, the curve shown in figure 3.4 depends on the ratio between translational and angular velocity. Thus, it cannot be used to determine the needed force and torque combination.
To solve this issue, microscopic displacement before the onset of sliding is considered. The threshold friction force can be described as:

$$\boldsymbol{f_f} = \mu_s p \int_{\text{contact area}} \frac{\delta y \boldsymbol{e}_y + r\delta\varphi \boldsymbol{e}_\varphi}{|\delta y \boldsymbol{e}_y + r\delta\varphi \boldsymbol{e}_\varphi|} d^2 r \tag{3.14}$$

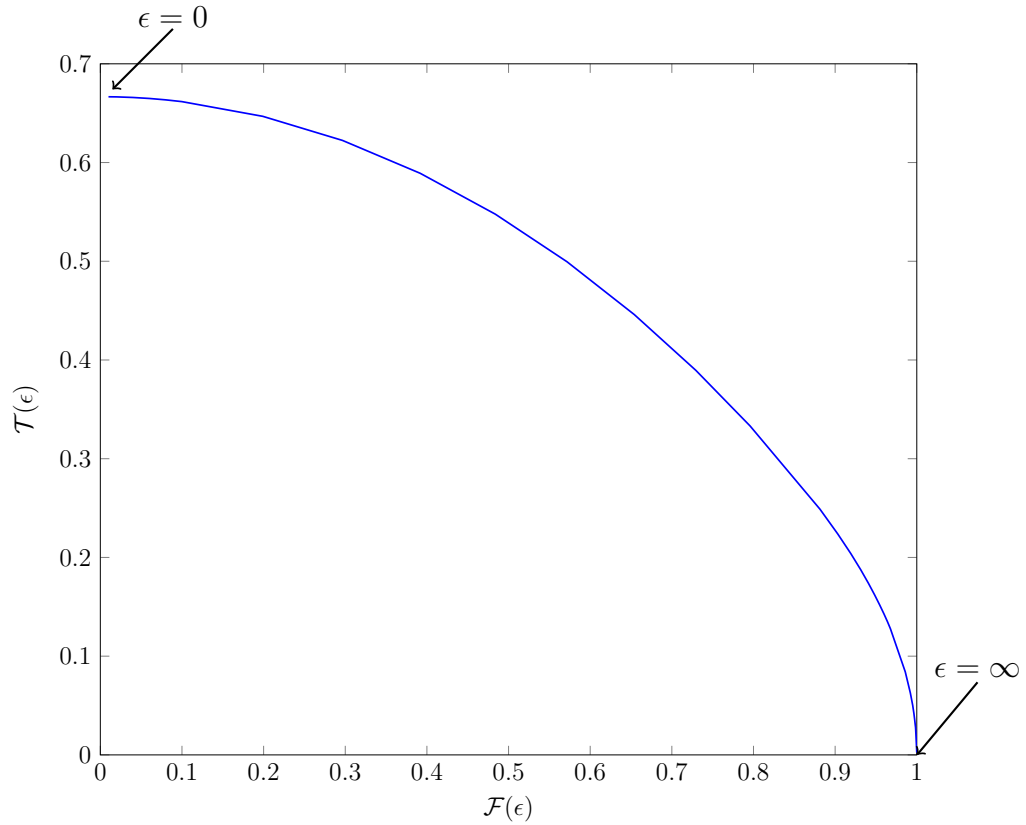

Figure 3.4: Graph of the coupling between $\mathcal{F}$ and $\mathcal{T}$.

where δy symbolises the microscopic translational displacement and $\delta\varphi$ the microscopic rotation [6]. $\boldsymbol{e}_y$ and $\boldsymbol{e}_\varphi$ are the directions of the microscopic displacements. In contrast to the dynamical friction coefficient μ_d, in the static case the static friction coefficient μ_s is used. In general μ_s is larger than μ_d and depends not only on the materials of the body and the surface but also on different conditions like contamination and aging that can be at atomic level [20]. Accordingly, the friction torque is:

$$\boldsymbol{\tau_f} = \mu_s p \int_{\text{contact area}} \boldsymbol{r} \times \frac{\delta y \boldsymbol{e}_y + r\delta\varphi \boldsymbol{e}_\varphi}{|\delta y \boldsymbol{e}_y + r\delta\varphi \boldsymbol{e}_\varphi|} d^2 r \tag{3.15}$$

With the help of the microscopic displacements a new ratio can be defined:

$$\gamma = \frac{\delta y}{R\delta\varphi} \tag{3.16}$$

However, Coulomb's model does not accurately define microscopic displacements. Thus, in the simulation the microscopic displacements were replaced with the first displacements unequal to zero.
Equations (3.14) and (3.15) can be solved to the same solution as in equation (3.10) and (3.12) [20]. The solution differs only in the used friction coefficient and the ratio. When a force and torque combination reaches the upper curve in figure 3.5, the object is set in motion. Generally that means it both slides and spins. However, after the initial onset of movement the needed force and torque combination to keep the object moving recedes to the lower curve in figure 3.5. Therefore it is important to determine the ratio ϵ that is valid immediately after the onset of movement. This can be done under the assumption that the externally applied force and torque only vary slightly in comparison to the difference between the force needed to set the object moving and to keep it moving [20]. Additionally to model the beginning of movement, the ratio ϵ is redefined to be a ratio of accelerations instead of velocities:

$$\epsilon = \frac{\dot{v}}{R\dot{\omega}} \tag{3.17}$$

With the help of this new definition it is possible to include directly the force and torque that set the object in motion. The translational acceleration is:

$$\dot{v} = \frac{1}{m}(f_{\text{applied}} - \mu_d f_n \mathcal{F}(\epsilon)) = \frac{f_n}{m}(\mu_s \mathcal{F}(\gamma) - \mu_d \mathcal{F}(\epsilon)) \tag{3.18}$$

where m is the mass of the sliding and spinning disk [6]. Accordingly, the angular acceleration can be computed by:

$$\dot{\omega} = \frac{f_n R}{I}(\mu_s \mathcal{T}(\gamma) - \mu_d \mathcal{T}(\epsilon)) \tag{3.19}$$

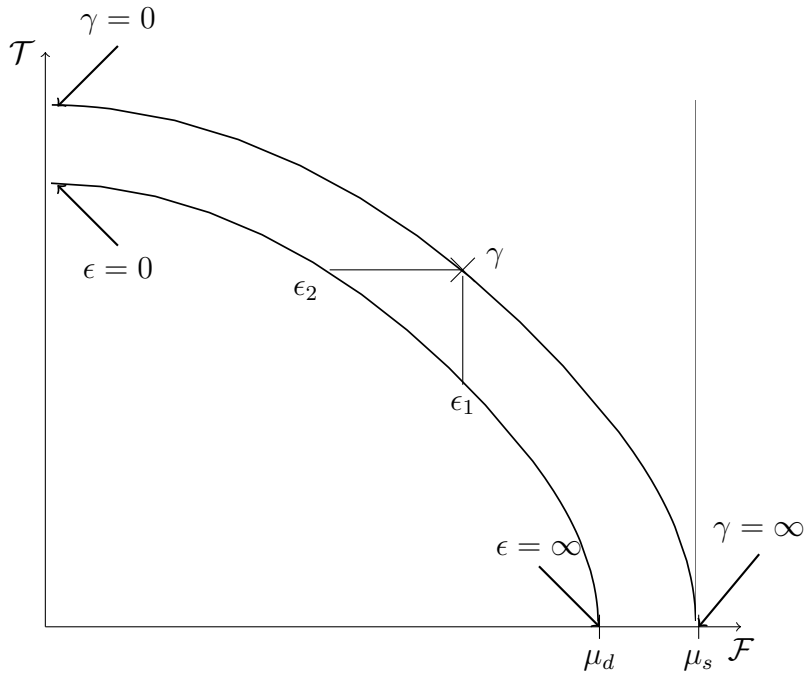

Figure 3.5: Construction of constraints to compute ϵ at the onset of sliding.

where I is the moment of inertia [6].
Combining equation (3.17) with (3.18) and (3.19) results in a new implicit definition of ϵ:

$$\epsilon = \frac{I}{mR^2} \frac{\mu_s \mathcal{F}(\gamma) - \mu_d \mathcal{F}(\epsilon)}{\mu_s \mathcal{T}(\gamma) - \mu_d \mathcal{T}(\epsilon)} \tag{3.20}$$

According to [20] this solution is not only valid for disks but also for any cylindrical bodies that have a circular contact area and the mass is distributed in a way that the pressure can be assumed to be constant.
As shown in figure 3.5 depending on the value of γ two values of ϵ can be chosen that act as constraints for equation 3.20. Both values ϵ_1 and ϵ_2 can range theoretically from zero to infinity, however it is possible to limit the values using

$$\mathcal{T}(\epsilon_1) \equiv \min\left(\frac{\mu_s}{mu_d}\mathcal{T}(\gamma), \mathcal{T}(0)\right) \tag{3.21}$$

and

$$\mathcal{F}(\epsilon_2) \equiv \min\left(\frac{\mu_s}{mu_d}\mathcal{F}(\gamma), \mathcal{F}(\infty)\right) \tag{3.22}$$

These values are needed to solve the non-linear equation. However the boundary values themselves are excluded from the solution in general [20]. Only

in the case of pure translational respectively pure rotational movement, the value of γ equals to both values of ϵ_1 and ϵ_2. In this case ϵ is equal to $\epsilon_1 = \epsilon_2 = \gamma$.

Chapter 4

Elasto-Plastic Model for Planar Motion

The coupling between force and torque presented in section 3 is based on the Coulomb friction model. To be able to judge the validity of the presented model a second model will be built. This second model will be used to draw comparisons between both concepts.
The method in section 4.1 was published in [1] and was developed to plan motion of a n-fingered robot. This model includes friction along both x- and y-direction as well as rotation around the z-axis. Both concepts were developed to be used with Coulomb's friction model. However, both concepts will be used with the elasto-plastic friction model. This adaptation is discussed in section 4.2.

4.1 Coupling of Sliding and Spinning Motion

In section 3 friction force and torque are coupled by the elliptic curve shown in figure 3.4. The approach for planar motion presented there was calculated analytically and is specific to the shape of the object.
In the following approach, the influence of the shape of the object is neglected. Furthermore, it is not based on analytical computations but uses previous experimental results [1]. Here the coupling is limited by the ellipsoid in figure 4.1. Force and torque combinations inside the ellipsoid do not result in sliding and spinning while combinations outside of the ellipsoid result in motion. As presented in [1] the ellipsoid is computed by:

$$\boldsymbol{f}^T \boldsymbol{A} \boldsymbol{f} = 1 \tag{4.1}$$

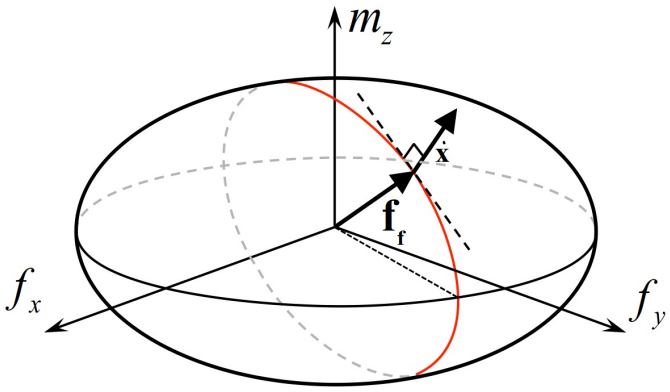

Figure 4.1: Three-dimensional ellipsoid that bounds the frictional force. Source:[1]

where $\boldsymbol{f} = [f_x, f_y, m_z]$ is a friction force vector and $\boldsymbol{A}$ is a matrix of the form:

$$\boldsymbol{A} = \begin{bmatrix} \frac{1}{f_C^2} & 0 & 0 \\ 0 & \frac{1}{f_C^2} & 0 \\ 0 & 0 & \frac{1}{(a \cdot R \cdot f_C)^2} \end{bmatrix} \tag{4.2}$$

where a is a constant that is chosen to be $a = 0.6$ in accordance with both [1] and the findings by [7]. Note also that f_C is the maximal friction force in the Coulomb model that is computed by:

$$f_C = \mu_d f_n$$

In the two-dimensional case, this approximate solution is compared to the analytic solution presented in chapter 3 in figure 4.2. Here the analytical solution is depicted in blue while the approximation is red. In this model the acting friction force is computed by:

$$\boldsymbol{f_f} = \frac{\boldsymbol{A}^{-1}\boldsymbol{v}}{\sqrt{\boldsymbol{v}^T \boldsymbol{A}^{-1} \boldsymbol{v}}} \tag{4.3}$$

where $\boldsymbol{v} = [v_x, v_y, \omega_z]^T$ is the velocity of the object.
Because of the usage of the Coulomb friction model, it is necessary to distinguish between static and dynamic friction. In the static friction it holds that:

$$\boldsymbol{f}^T \boldsymbol{A} \boldsymbol{f} < 1 \tag{4.4}$$

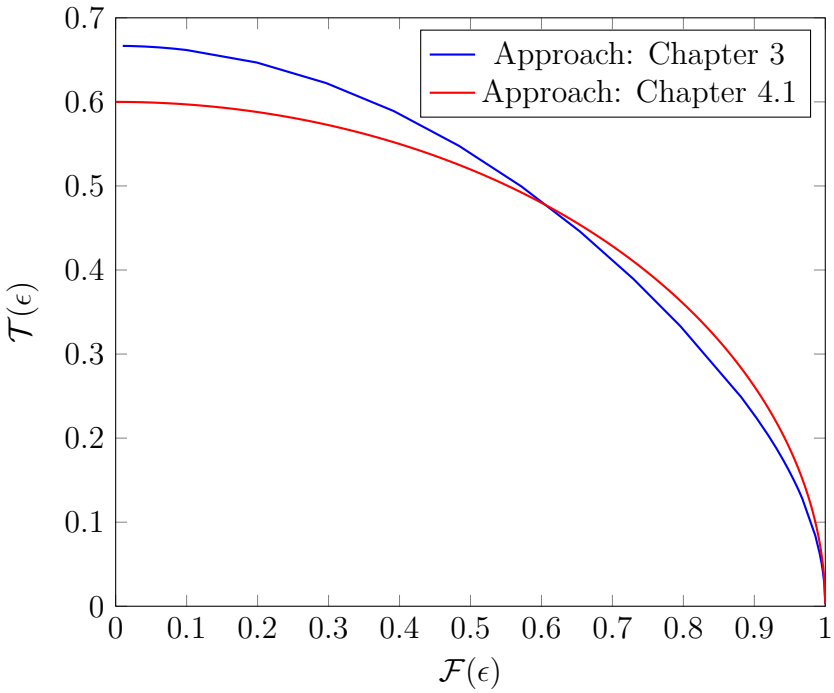

Figure 4.2: Comparison of elliptic curves used in different approaches.

Here the limiting ellipsoid does not come into play so that the motion can be computed using the following equation:

$$\begin{bmatrix} m & 0 & 0 \\ 0 & m & 0 \\ 0 & 0 & I \end{bmatrix} \dot{\boldsymbol{v}} = \boldsymbol{f_{applied}} - \boldsymbol{f} \tag{4.5}$$

where $\dot{\boldsymbol{v}}$ is the acceleration of the object and I the inertia of the object. However, in the dynamic case the friction force and torque has to be limited. Therefore, instead of using the force vector $\boldsymbol{f}$ the limited force vector $\boldsymbol{f_f}$ is used. Thus equation (4.5) is changed to:

$$\begin{bmatrix} m & 0 & 0 \\ 0 & m & 0 \\ 0 & 0 & I \end{bmatrix} \dot{\boldsymbol{v}} = \boldsymbol{f_{applied}} - \boldsymbol{f_f} = \boldsymbol{f_{applied}} - \frac{\boldsymbol{A}^{-1}\boldsymbol{v}}{\sqrt{\boldsymbol{v}^T\boldsymbol{A}^{-1}\boldsymbol{v}}} \tag{4.6}$$

4.2 Implementation

The classical translational Coulomb friction as given in equation 2.1 can be rewritten as:

$$f_f = -\mu_d f_n \text{sign}(\dot{x}) \tag{4.7}$$
$$= -f_C \text{sign}(\dot{x}) \tag{4.8}$$

In the planar case this equation 4.7 changes to equation 4.3. A different representation of equation (4.7) is:

$$\boldsymbol{f_f} = \mu_d \frac{\boldsymbol{A}^{-1}\boldsymbol{v}}{\sqrt{\boldsymbol{v}^T \boldsymbol{A}^{-1}\boldsymbol{v}}} \tag{4.9}$$

where $\boldsymbol{A}$ is changed to:

$$\boldsymbol{A} = \begin{bmatrix} \frac{1}{f_C^2} & 0 & 0 \\ 0 & \frac{1}{f_C^2} & 0 \\ 0 & 0 & \frac{1}{(a \cdot R \cdot f_n)^2} \end{bmatrix} \tag{4.10}$$

To be able to include the planar motion in the elasto-plastic model it is necessary to enhance the model as presented in section 2.5. The Coulomb friction is bounded by the Coulomb friction force f_C. The counterpart in the elasto-plastic model that limits the friction force is the steady-state friction force $f_s s(\dot{x})$. This force has to be changed to include planar motion. Therefore it is necessary to change equation (2.14) with the help of equations (2.2) and (2.7) to resemble equation (4.7) more closely:

$$f_{ss}(\dot{x}) = \left[(\mu_s f_n - \mu_d f_n) e^{-|\dot{x}|^2/\dot{x}_s^2} + \mu_d f_n \right] \text{sign}(\dot{x}) \tag{4.11}$$
$$= \left[(\mu_s - \mu_d) e^{-|\dot{x}|^2/\dot{x}_s^2} + \mu_d \right] f_n \text{sign}(\dot{x}) \tag{4.12}$$

This allows to include planar motion in the following way:

$$\boldsymbol{f_{ss}} = \left[(\mu_s - \mu_d) e^{-\left(\frac{|\boldsymbol{v}|}{\boldsymbol{v}_s}\right)^2} + \mu_d \right] \frac{\boldsymbol{A}^{-1}\boldsymbol{v}}{\sqrt{\boldsymbol{v}^T \boldsymbol{A}^{-1}\boldsymbol{v}}} \tag{4.13}$$

where $\boldsymbol{A}$ stays the same as given in equation (4.10).

Chapter 5

Discussion

This chapter is structured as follows. The beginning focuses on one-dimensional motion. Therefore, the following three exemplary test cases are presented and discussed.

- A general translational test case without focus on a specific friction phenomenon.
- A test case that focuses on the presliding prediction of the friction models.
- A so-called "Rabinowicz test" that concentrates on the simulation of the stick-slip effect.

Following one-dimensional motion, planar motion models are simulated. To simulate planar motion, an impulse-like force and torque is applied on four different models:

- Coulomb friction model with planar motion model by Shi.
- Coulomb friction model with planar motion model by Farkas.
- Enhanced elasto-plastic model with planar motion model by Shi.
- Enhanced elasto-plastic model with planar motion model by Farkas.

5.1 One-dimensional Movement

5.1.1 Translational test

In chapter 2 different models are presented that focus upon various friction phenomena. Differences and similarities in the models will be discussed in

this chapter.
To show basic differences in the models, a simple test case is used. In this test an object is pushed across a flat surface to simulate the friction force as depicted in figure 2.1. In this scenario, the dynamics are computed using Newton's second law:

$$F = m\dot{v} \tag{5.1}$$

were $\dot{v}$ is the acceleration of the object and F the sum of all forces, here the externally applied force $f_{applied}$ and the resulting friction force f_f. This results in:

$$f_{applied} - f_f = m\dot{v} \tag{5.2}$$

The parameters used in this test are listed in table 5.1 and the applied force is shown in black in figure 5.1. The simplest friction model used in this test case is the Coulomb model with enhancements described in section (2.4) and (2.5). It can be seen that the friction force - represented in red - follows the applied force until the friction force is limited by the Coulomb friction constant. This results in a discontinuity in the friction force. The velocity-dependent viscous friction coefficient of the enhanced Coulomb model has only a marginal influence in this example.

This discontinuity is avoided in Dahl's model because it contains one continuous state. Thus the resulting friction force of Dahl's model is a smooth curve. This smooth transition between the static and dynamic friction case is a result of the model's ability to predict presliding displacement. It is depicted with the green line in figure 5.1.
However, when there is a transition from dynamic to static friction, Dahl's model is not able to model this correctly. For example in figure 5.1, all other models predict zero friction force after 1.2 seconds, but Dahl's model predicts an oscillating force. This can result in a drifting motion but is not

Table 5.1: Parameters used in one-dimensional test case.

Parameter	Formula symbol	Value
mass	m	$10\,\mathrm{kg}$
Coulomb friction coefficient	f_C	$1\,\mathrm{N}$
maximal static friction level	f_{max}	$1.5\,\mathrm{N}$
critical velocity for Stribeck effect	v_s	$10^{-3}\,\mathrm{m/s}$
break-away displacement	z_{ba}	$8 \cdot 10^{-6}\,\mathrm{m}$
contact stiffness	σ_0	$10^5\,\mathrm{N/m}$
tangential damping	σ_1	$1000\,\mathrm{Ns/m}$
viscous friction coefficient	σ_2	$0.4\,\mathrm{Ns/m}$

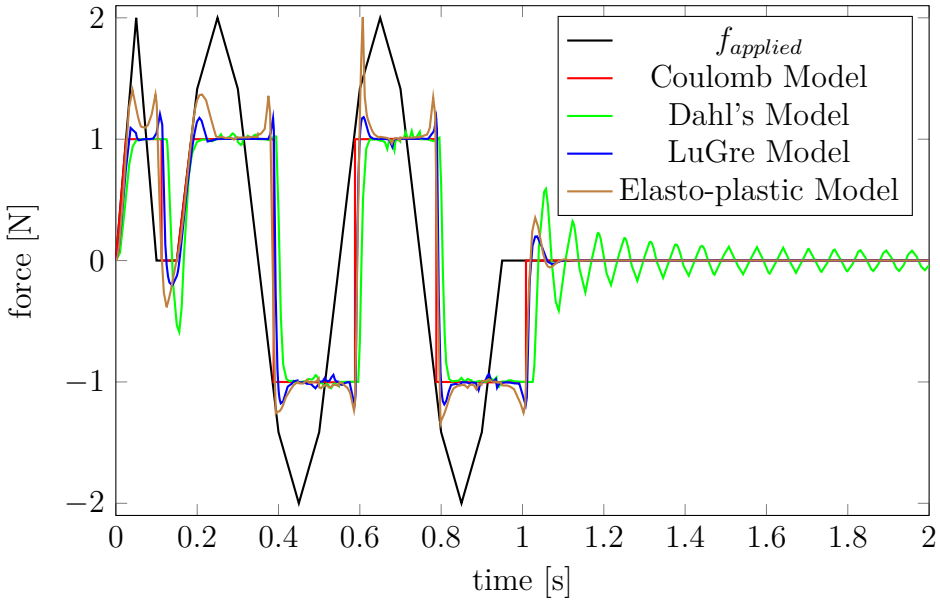

Figure 5.1: Plot of applied force $f_{applied}$ and various resulting friction forces f_f.

noticeable in this test because of the chosen parameters. Although Dahl's model predicts a slightly different friction force, the difference compared to the enhanced Coulomb model is not significant enough to lead to different velocities in this particular test case as seen in figure 5.3.
When using the LuGre model in the same testing conditions, this oscillating force is not noticeable. The results of the test case using the LuGre model are depicted in figure 5.1 in blue. The further advancement of the LuGre model compared to Dahl's model is the extension to include the Stribeck effect described in section 2.2. Before the object moves, first the friction force increases above the Coulomb friction coefficient until the object moves. After the onset of movement the friction force decreases because of the Stribeck effect. At higher velocities the friction force increases again. This behaviour can be witnessed in figure 5.2 that is an enlargement of the figure 5.1.
Finally, the results using the elasto-plastic model are depicted in figure 5.1 in brown. In this test case, no major differences between the results of the LuGre model and the elasto-plastic model are noticeable. However, at the onset of motion the simulated friction force differs because of differences in modelling. This can be observed at the time 0.6 s in figure 5.1 for example.

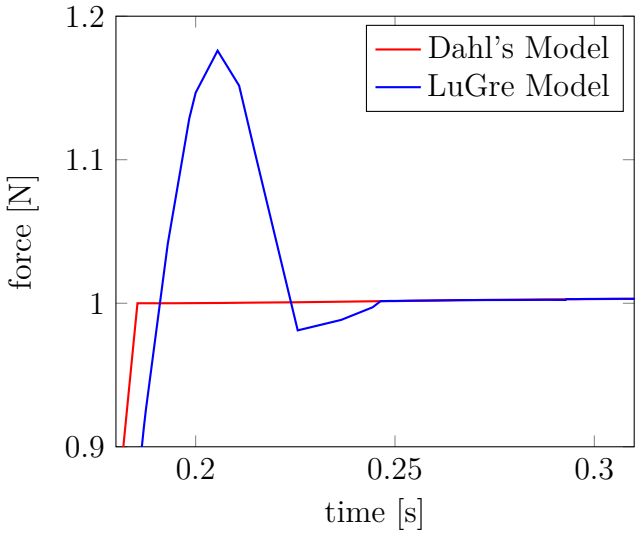

Figure 5.2: Enlarged plot of figure 5.1 to depict Stribeck effect in LuGre model compared to Coulomb's model.

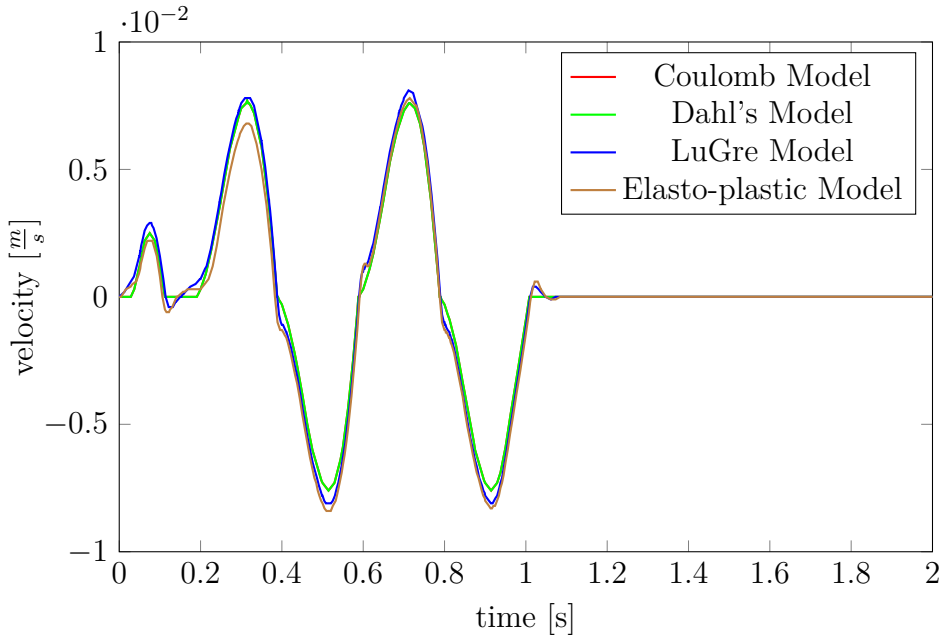

Figure 5.3: Resulting velocities in one-dimensional test case.

5.1.2 Presliding test case

Dahl's model, LuGre model and the elasto-plastic model include presliding. However, it is modelled differently. To analyse the resulting differences, in [5] a test case was proposed. In this test, a particular force is applied that is provided in figure 5.4. In the beginning there is a peak above the Coulomb friction force f_C. Later on there are oscillations below f_C. Thus, it is expected that only presliding displacement is simulated. In table 5.2 the used parameters are shown. As seen in figure 5.6 all three models are able to show presliding behaviour. However, both Dahl's model and the LuGre model simulate drift that is not expected because of the applied force. The drift is more pronounced in Dahl's model as the friction force is larger as shown in figure 5.5. The elasto-plastic model shows the displacement as expected

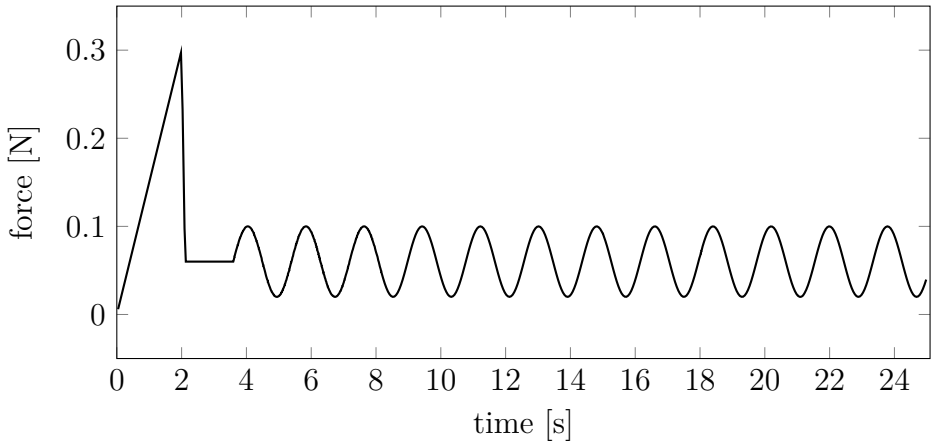

Figure 5.4: Plot of applied force $f_{applied}$ in presliding test case.

Table 5.2: Parameters used in presliding test case.

Parameter	Formula symbol	Value
mass	m	$1\,\mathrm{kg}$
Coulomb friction coefficient	f_C	$0.2058\,\mathrm{N}$
maximal static friction level	f_{max}	$0.3087\,\mathrm{N}$
critical velocity for Stribeck effect	v_s	$10^{-3}\,\mathrm{m/s}$
break-away displacement	z_{ba}	$0.0062\,\mathrm{m}$
contact stiffness	σ_0	$23.66\,\mathrm{N/m}$
tangential damping	σ_1	$2.8034\,\mathrm{Ns/m}$
viscous friction coefficient	σ_2	$0\,\mathrm{Ns/m}$

because of the input force: it shows typical presliding oscillations without predicting drift.

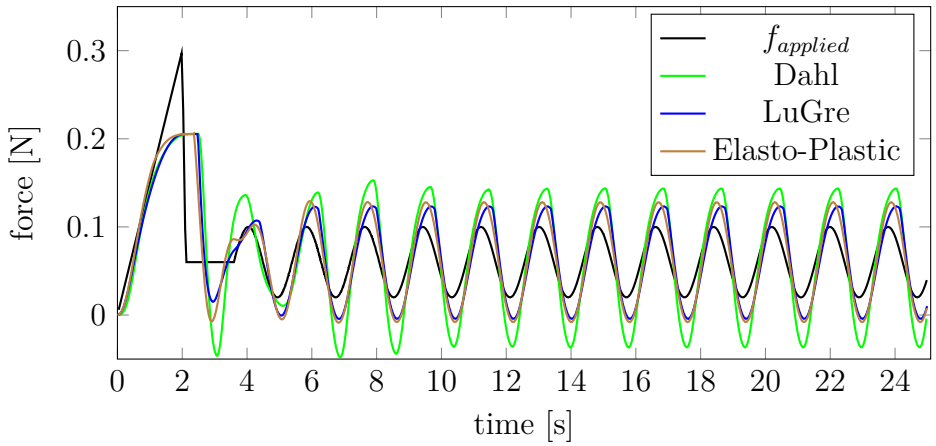

Figure 5.5: Plot of resulting friction forces f_f in presliding test case.

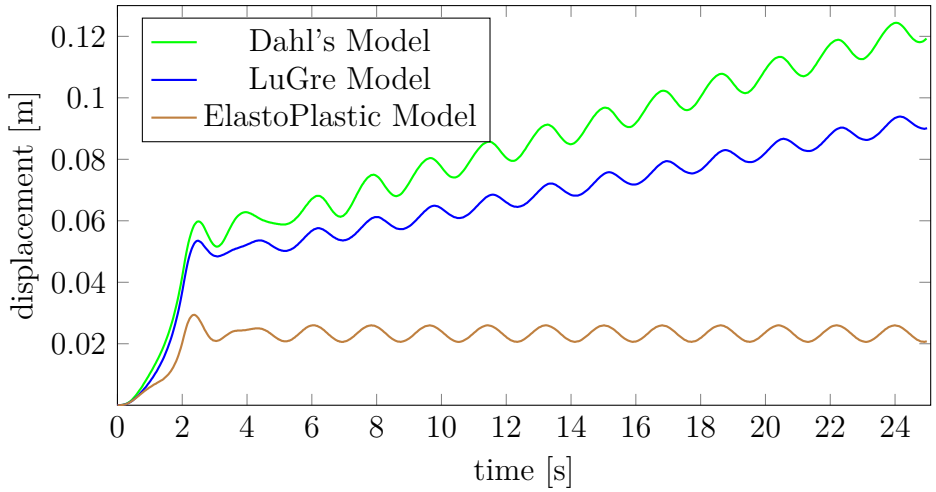

Figure 5.6: Plot of predicted displacements in presliding test case.

5.1.3 Rabinowicz test case

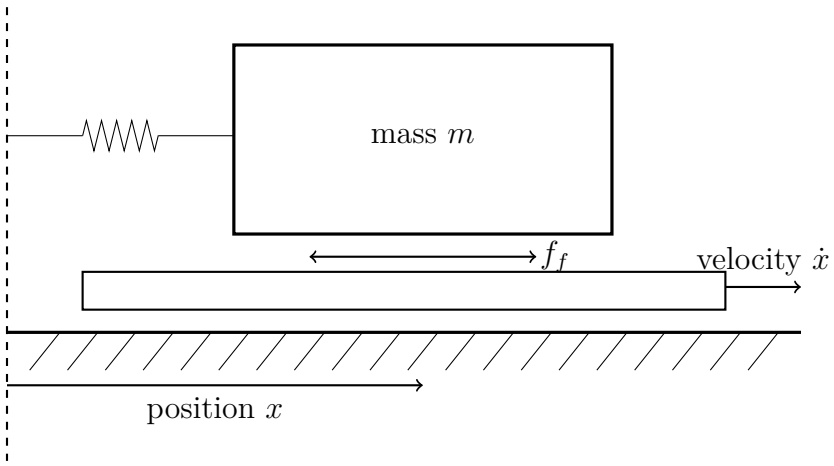

Figure 5.7: Schematic view of the Rabinowicz test case.

The Rabinowicz test case was first presented in [21] in 1956. Since then it has been accepted as a test for friction models to test stick-slip behaviour [11]. In the Rabinowicz test case, a slab moves with a constant velocity below an object with the mass m. The object is connected to the inertial reference frame with a spring as seen in figure 5.7. In this test case the velocity was chosen to be: $\dot{x} = 0.5\,\mathrm{m/s}$. Further used parameters can be found in table 5.3.
Concerning the stick-slip effect, it is possible to distinguish two groups of models.

1. Models not covering the stick-slip effect, like the Coulomb model and Dahl's model

Table 5.3: Parameters used in Rabinowicz test case.

Parameter	Formula symbol	Value
mass	m	$20\,\mathrm{kg}$
stiffness of spring	k	$10\,\mathrm{N/m}$
Coulomb friction coefficient	f_C	$98.1\,\mathrm{N}$
maximal static friction level	f_{max}	$117.72\,\mathrm{N}$
critical velocity for Stribeck effect	v_s	$0.05\,\mathrm{m/s}$
contact stiffness	σ_0	$98100\,\mathrm{N/m}$
tangential damping	σ_1	$780\,\mathrm{Ns/m}$
viscous friction coefficient	σ_2	$0\,\mathrm{Ns/m}$

2. Models including the stick-slip effect, for example the LuGre model and the elasto-plastic model

This clear distinction is verified in this test case. The Coulomb model and Dahl's model approach a constant friction force as seen in figure 5.8. Because of this similarity, both models predict comparable velocities and displacements.
The second group simulates a later onset of sliding as shown in figure 5.9. Until time $t = 25\,\mathrm{s}$ the object sticks on the moving slab. Furthermore, both the LuGre model and the elasto-plastic model predict a return to stiction again at time $t = 30\,\mathrm{s}$ and $t = 43\,\mathrm{s}$.
In figure 5.10, the simulated displacements are shown. There, it is possible to see that stiction results in constant motion because of the motion of the slab.

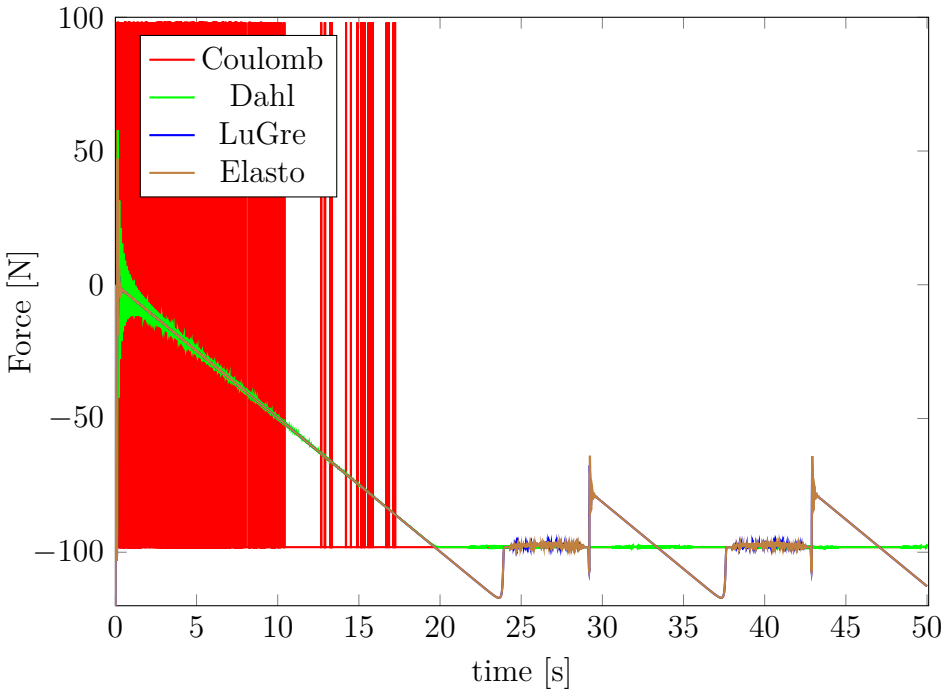

Figure 5.8: Plot of predicted frictional forces in Rabinowicz test case.

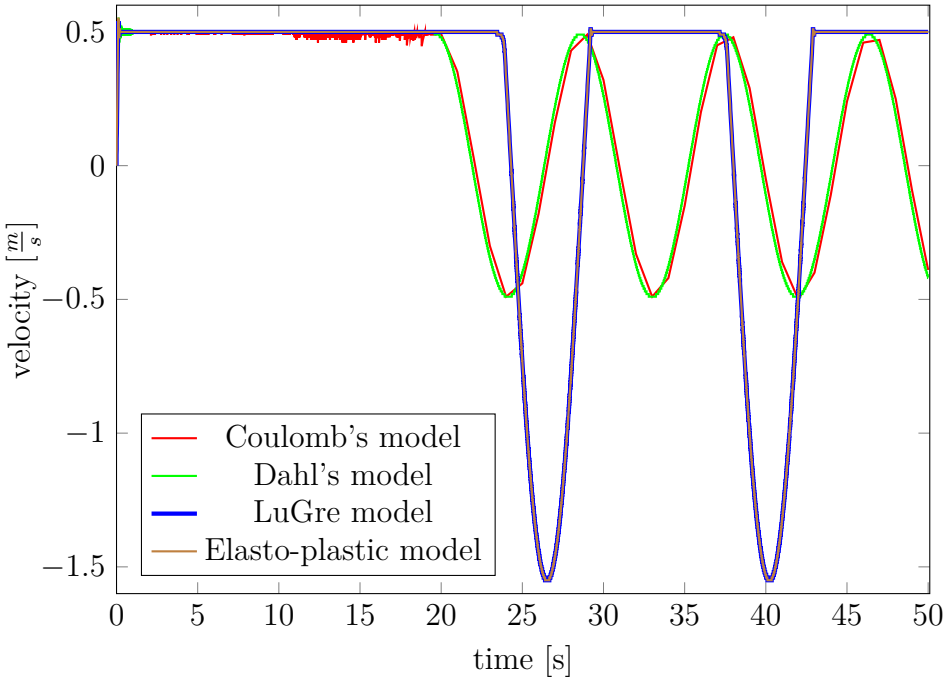

Figure 5.9: Plot of predicted velocities in Rabinowicz test case.

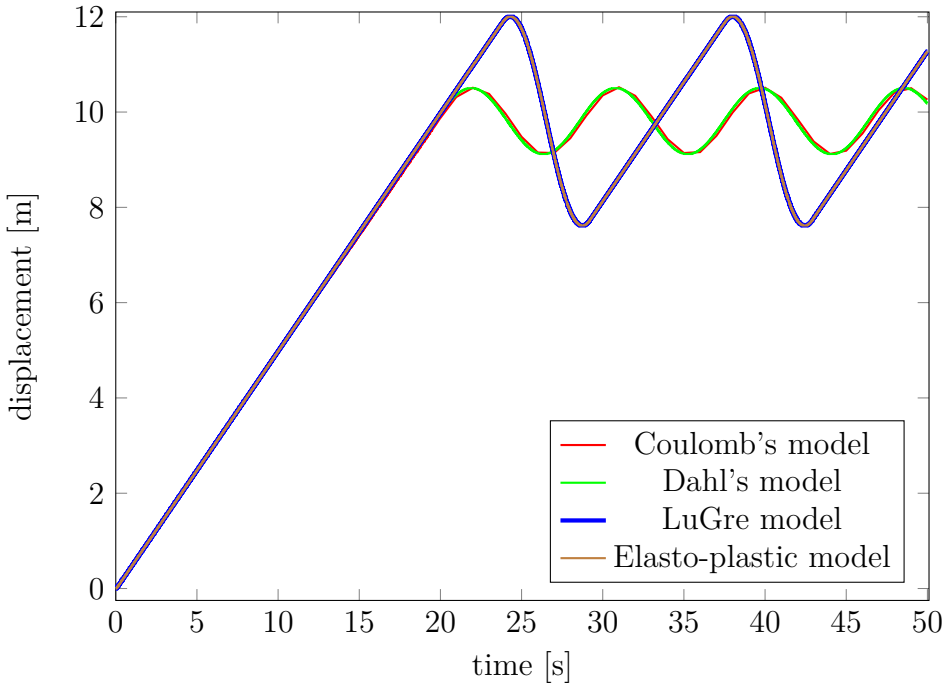

Figure 5.10: Plot of predicted displacements in Rabinowicz test case.

5.2 Planar Movement

In the following, different approaches to model planar motion will be compared using the Coulomb model and the adapted elasto-plastic model.
In this comparison the applied force includes both forces and torque as depicted in figure 5.11. The used parameters can be seen in table 5.4.
At first, the planar motion is modelled according to the Coulomb model. In

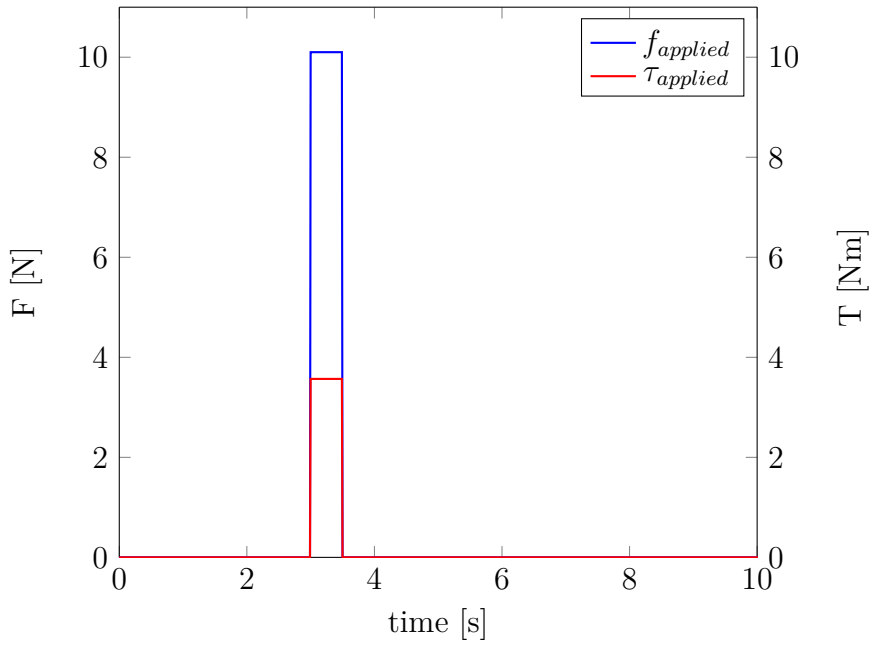

Figure 5.11: Applied force and torque combination for comparison of planar motion.

figure 5.12 the simulated translational velocities are displayed using the two different approaches described in section 4.2 and section 3.1. The associated rotational velocities are shown in figure 5.13.
Then the motion is modelled using the enhanced elasto-plastic model. The translational velocities are shown in figure 5.14 and the rotational velocities are depicted in figure 5.15. When using the Coulomb model (figures 5.12, 5.13), the planar motion differs in magnitude but the derivatives are mostly the same. Comparing the motions modelled with the enhanced elasto-plastic model, the motions shown in figures 5.14 and 5.15 are nearly identical. However, there is a difference in magnitude in the rotational motions when comparing the Coulomb model and the enhanced elasto-plastic model.

Therefore, it is possible to conclude that both approaches in modelling

Table 5.4: Parameters used in planar test case.

Parameter	Formula symbol	Value
mass	m	$2.0106\,\mathrm{kg}$
inertia	I	$0.0064\,\mathrm{m^2kg}$
Coulomb friction coefficient	f_C	$7.1007\,\mathrm{N}$
maximal static friction level	f_{max}	$7.4952\,\mathrm{N}$
critical velocity for Stribeck effect	v_s	$10^{-3}\,\mathrm{m/s}$
break-away displacement	z_{ba}	$8 \cdot 10^{-8}\,\mathrm{m}$
contact stiffness	σ_0	$100000\,\mathrm{N/m}$
tangential damping	σ_1	$1000\,\mathrm{Ns/m}$
viscous friction coefficient	σ_2	$0.4\,\mathrm{Ns/m}$

planar motion result in similar frictional behaviour in this scenario. The approach described in section 4.1 is an approximate approach as it does not rely on the form of the object for example. Because of this simplification, it is more easily possible to include more objects as shown in [1]. This results in some flexibility. Compared to this, the approach described in section 4.2 is more restrained. However, the approach in section 4.2 is not an approximation but based on analytical solutions.
In this test case the friction behaviour is modelled for a flat disk. As described in [9], the formulas for $\mathcal{F}(\epsilon)$ (equation (3.11)) and $\mathcal{T}(\epsilon)$ (equation (3.13)) have to be changed according to the object. However, these formulas can only be analytically described in few cases; one of which is a flat disk. The results of this test are depicted in figures 5.12 - 5.15. When comparing both approaches from section 4.1 and 4.2, the most noticeable difference is the magnitude of the resulting translational velocity when the friction force is modelled based on the Coulomb model.

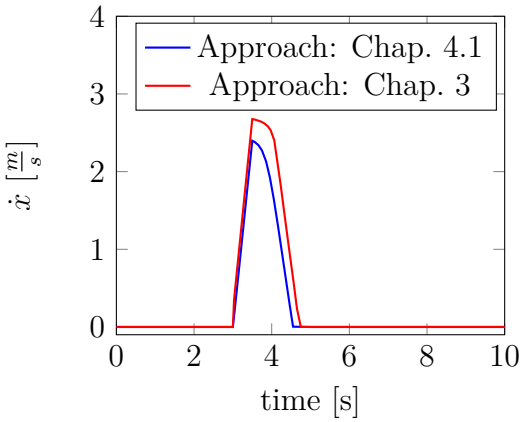

Figure 5.12: Resulting translational velocity of planar motion with Coulomb model.

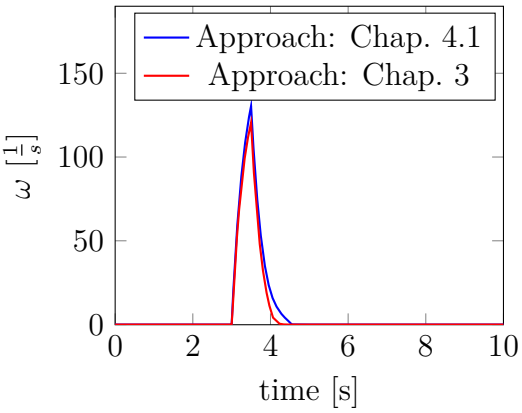

Figure 5.13: Resulting rotational velocity of planar motion with Coulomb model.

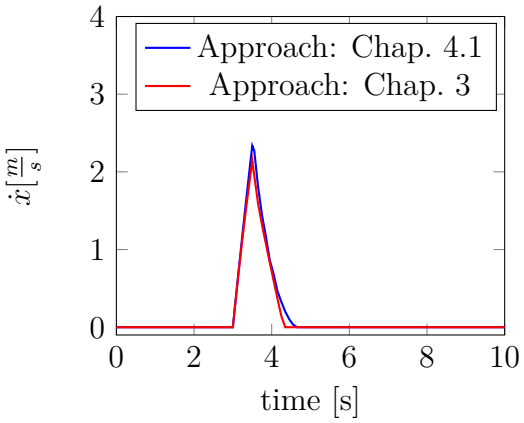

Figure 5.14: Resulting translational velocity of planar motion modelled with enhanced elasto-plastic model.

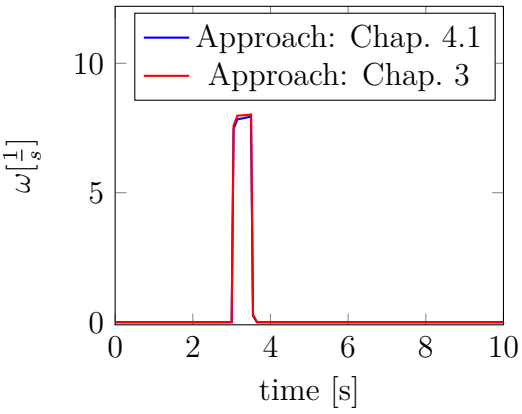

Figure 5.15: Resulting rotational velocity of planar motion modelled with enhanced elasto-plastic model.

Chapter 6

Conclusion

In this thesis project various one-dimensional friction models were modelled and compared in different scenarios. In the test cases it is apparent that different friction models result in different outcomes - especially at low velocities. Using two friction models exemplary, planar motion was simulated with the help of two different theoretical approaches.
At low velocities, it is especially important to simulate when an object sticks again after motion. In this thesis it was shown that the LuGre friction model and especially the elasto-plastic friction model allow such precise modelling for one-dimensional motion. This is because both simulate stiction and the stick-slip behaviour.
For manipulation tasks it is also important to model planar motion. Like mentioned above, two different approaches were implemented. The theoretical approach presented in chapter 3 is more precise as it depends on analytical solutions. However, that approach is quite specific to the shape of the object and has to be solved for every shape separately. The second approach was presented in chapter 4.2 is less specific to the shape of the object. This results from an approximation done in the theoretical concept. To sum up, it is necessary to gauge the advantages and disadvantages of both approaches for a specific application.
Recently, friction models are included in different manipulation tasks. One example is to replace pick-and-place operations. Instead an object is pushed across a flat surface; it is no longer needed to lift up the object. To be able to predict the motion of the pushed object, friction models like the LuGre and elasto-plastic models are needed because they allow precise friction modelling at low velocities.
Because of this, suggestions for future works are:

- To be able to judge the discrepancies resulting from the approximation, it is necessary to do friction experiments for planar motion to

gain a complete experimental data set to allow for validation of planar frictional behaviour. This would allow to eliminate the uncertainty in planar modelling.

- Do the models have to be changed to allow for real-time simulation?
- Implementing planar frict?ion models in robotic applications.

Bibliography

[1] Jian Shi, J Zachary Woodruff, Paul B Umbanhowar, and Kevin M Lynch. Dynamic in-hand sliding manipulation. *IEEE Transactions on Robotics*, 2017.

[2] Andrea Bisoffi, Mauro Da Lio, Andrew R Teel, and Luca Zaccarian. Global asymptotic stability of a pid control system with coulomb friction. *arXiv preprint arXiv:1609.09103*, 2016.

[3] Vincent Hayward, Brian SR Armstrong, Friedhelm Altpeter, and Pierre E Dupont. Discrete-time elasto-plastic friction estimation. *IEEE transactions on control systems technology*, 17(3):688–696, 2009.

[4] Robert D Howe and Mark R Cutkosky. Practical force-motion models for sliding manipulation. *The International Journal of Robotics Research*, 15(6):557–572, 1996.

[5] Pierre Dupont, Vincent Hayward, Brian Armstrong, and Friedhelm Altpeter. Single state elastoplastic friction models. *IEEE Transactions on automatic control*, 47(5):787–792, 2002.

[6] Sílvio R Dahmen, Zénó Farkas, Haye Hinrichsen, and Dietrich E Wolf. Macroscopic diagnostics of microscopic friction phenomena. *Physical Review E*, 71(6):066602, 2005.

[7] Zénó Farkas, Guido Bartels, Tamás Unger, and Dietrich E Wolf. Frictional coupling between sliding and spinning motion. *Physical review letters*, 90(24):248302, 2003.

[8] AA Kireenkov. Generalized two-dimensional model of sliding and spinning friction. In *Doklady Physics*, volume 55, pages 186–190. Springer, 2010.

[9] Patrick D Weidman and Chetan P Malhotra. On the terminal motion of sliding spinning disks with uniform coulomb friction. *Physica D: Nonlinear Phenomena*, 233(1):1–13, 2007.

[10] Phil R Dahl. A solid friction model. Technical report, DTIC Document, 1968.

[11] Ettore Pennestrì, Valerio Rossi, Pietro Salvini, and Pier Paolo Valentini. Review and comparison of dry friction force models. *Nonlinear Dynamics*, 83(4):1785–1801, 2016.

[12] YF Liu, J Li, ZM Zhang, XH Hu, and WJ Zhang. Experimental comparison of five friction models on the same test-bed of the micro stick-slip motion system. *Mechanical Sciences*, 6(1):15, 2015.

[13] Henrik Olsson, Karl J Åström, C Canudas De Wit, Magnus Gäfvert, and Pablo Lischinsky. Friction models and friction compensation. *European journal of control*, 4(3):176–195, 1998.

[14] Brian Armstrong-Helouvry. *Control of machines with friction*, volume 128. Springer Science & Business Media, 2012.

[15] Brian Armstrong-Hélouvry. *Control of Machines with Friction*, volume 128. Springer Science & Business Media, 1991.

[16] Karl Johan Åström and Carlos Canudas-de Wit. Revisiting the lugre friction model. *IEEE control Systems*, 28(6):101–114, 2008.

[17] Jan Swevers, Farid Al-Bender, Chris G Ganseman, and Tutuko Projogo. An integrated friction model structure with improved presliding behavior for accurate friction compensation. *IEEE Transactions on automatic control*, 45(4):675–686, 2000.

[18] Philip R Dahl. Solid friction damping of mechanical vibrations. *AIAA journal*, 14(12):1675–1682, 1976.

[19] Pierre Dupont, Brian Armstrong, and Vincent Hayward. Elasto-plastic friction model: contact compliance and stiction. In *American Control Conference, 2000. Proceedings of the 2000*, volume 2, pages 1072–1077. IEEE, 2000.

[20] Dietrich E Wolf, Silvio R Dahmen, and Haye Hinrichsen. Solid friction: Spinning at the onset of sliding. *International Journal of Modern Physics B*, 21(23n24):4158–4163, 2007.

[21] Ernest Rabinowicz. Stick and slip. *Scientific American*, 194(5):109–118, 1956.